# Functional Characterization of Cardiac Actin Mutants Causing Hypertrophic (p.A295S) and Dilative Cardiomyopathy (p.R312H and p.E361G)

**Constanze Erdmann**
Department of Anatomy and Molecular Embryology, Ruhr-University

**Roua Hassoun**
Molecular and Experimental Cardiology,Bergmannsheil and St. Josef Hopsital, Ruhr-University,

**Sebastian Schmitt**
Institute for Structural Biology; University of Bonn

**Setsuko Fujita-Becker**
University of Heidelberg Bioquant

**Antonina J. Mazur**
University Hospital of Wales Cellular Pathology Department

**Andreas Mügge**
Molecular and Experimental Cardiology, Bergmannsheil and St. Josef Hospital, Ruhr-University

**Rasmus R. Schröder**
University of Heidelberg Bioquant

**Matthias Geyer**
Institute of Structural Biology, University of Bonn

**Kornelia Jaquet**
Molecular and Experimental Cardiology, Bergmannsheil and St. Josef Hospital, Ruhr-University

**Hans Georg Mannherz** ( hans.g.mannherz@rub.de )
Department of Anatomy and Molecular Embryology https://orcid.org/0000-0001-8158-5722

**Original Article**

**Keywords:** ATPase, cardiac actin, calcium, cardiomyopathies, myosin subfragment 1, myosin binding protein C

**Posted Date:** February 2nd, 2021

**DOI:** https://doi.org/10.21203/rs.3.rs-159358/v1

# Abstract

The human mutant cardiac α-actins p.A295S or p.R312H (plus p.R312K) and p.E361G correlated with hypertrophic or dilative cardiomyopathy, respectively, were expressed by using the *baculovirus/Sf21* insect cell system. After purification their biochemical and cell biological properties were analysed and compared to wild type (wt) cardiac actin identically obtained or conventionally isolated from bovine hearts. DNase I inhibition and their polymerization behaviour indicated that all c-α-actins had maintained their native state. Cardiomyopathy type specific differences were observed except for the p.R312K mutant, which behaved like wt c-α-actin. The extent of myosin-S1 ATPase stimulation by the c-actin variants and its $Ca^{2+}$-sensitivity after decoration with tropomyosin (cTm) and troponin complex (cTn) varied being highest for the HCM p.A295S and lower for both DCM mutants. Similar $Ca^{2+}$-sensitivity differences were observed by recording the fluorescence increase of pyrene-cTm in the absence or presence of myosin-S1 and/or the actin-binding N-terminal fragment of cardiac myosin binding protein C (N-cMyBP-C). Transfection experiments showed the incorporation of the c-actin variants into existing cytoskeletal elements of non-muscle cells. Wt and p.A295S c-α-actin preferably incorporated into the microfilament system and p.R312H and p.E361G into the submembranous actin network of MDCK cells. Transduction of neonatal rat cardiomyocytes with adenoviral constructs coding for HA-tagged c-α-actins showed their incorporation into thin filaments of nascent sarcomeric structures at their plus ends (Z-lines) except the p.E361G mutant, which preferably incorporated at the minus ends. Our data indicate functional differences of the c-α-actins that may be causative for the different cardiomyopathy phenotypes.


# Introduction

Cardiomyopathies (CM) are generally characterized by electric dysfunction, hypertrophy or dilation. Hypertrophic cardiomyopathy (HCM) is characterized by an eccentric left ventricular wall thickness accompanied by an increased stiffness of the cardiac muscle resulting in reduced ventricular filling during diastole. Dilated cardiomyopathy (DCM) is characterized by fibrosis and enlarged left and/or right ventricle with a reduced ejection volume during systole. Whereas HCM has a genetic background in about 90% of all cases with a prevalence of 1:500 in the general population, DCM is in only 20% genetically based with a prevalence of 1: 2,500. In the remaining 80% of all cases DCM develops as a complication of bacterial or viral infections, adverse life style, alcoholism, drug abuse or chemotherapy [53,54,66].

The genetically caused (familial) cardiomyopathies (CM) are caused in the vast majority by mutations in genes encoding sarcomeric [3,53] or cytoskeletal proteins [15,36], i.e. actin binding proteins. About 1,400 different mutations causative for HCM or DCM have so far been described. In HCM the most frequently affected sarcomeric proteins are the ß-myosin heavy chain and the myosin binding protein C (MyBP-C) [9,53,54]. It has been observed that mutations in genes of cytoskeletal proteins occur more frequently in familial DCM, in particular of components of the intercalated disc [15]. In about 20% of the acquired DCM cases, titin gene truncations are observed as *de novo* mutations [23]. But mutations leading to HCM or DCM have been identified also within the same gene like for instance in the ACTC gene coding for cardiac

α-actin (c-α-actin). Typically, the CM mutations act in a dominant negative manner and are therefore in most cases single-allelic. Consequently, it is supposed that the mutated protein overrides in a poisonous manner the counterpart of the healthy allele [3,39]. The expression dosage of the mutant and healthy allele are usually equal, but deviations will contribute to the resulting phenotype [36,56].

Mutations of the c-α-actin gene are with an incidence of 4–6% an infrequent finding in patients with familial HCM, the incidence may be even lower in patients with familial DCM [11,17,18,39,44]. This low incidence is in contrast to myopathies of skeletal muscle, which are caused to about 30% by mutations of the skeletal muscle actin gene (ACTA1) [36,46].

The first mutations of cardiac α-actin, which were found in DCM patients, were the p.R312H and p.E361G mutations located in subdomain 4 and 1 of actin, respectively [44]. The first actin mutants causing HCM were p.H90Y and p.R97C both located in subdomain 1 [45]. Subsequently, a number of further mutations in c-α-actin were described that lead to HCM [46]. Presently 40 mutations have been identified [36], of which 14 different HCM and two DCM causing mutations are known [16], most of which are located within subdomains 1 and 4. Figure 1 shows the 3D structural model of G-actin [27] indicating the positions of the c-α-actin point mutations correlated to HCM and DCM.

Dysfunctions connected to the different mutations largely depend on the type of amino acid exchange, their localisation within the actin molecule, and the effect on the interaction with specific binding partners [45,46,63]. Thus for example, mutations in subdomain 4 affect the stability of the actin filament, though subdomain localization appears not decisive for HCM or DCM development [6,9,11,18,39]. The development of a certain cardiomyopathy phenotype does not follow a single pathway. It is complicated by the fact that missense mutations in many different sarcomeric proteins can lead to the same disease phenotype and conversely point mutations at different locations in the same protein can induce diverse outcomes [66,56]. Therefore for the development of a specific disease phenotype it may be decisive how a mutation affects the overall architecture and/or functionality of the sarcomere or the whole cardiomyocyte by for instance its modified interactions with different binding partners. On the way to such an understanding it is however necessary to analyse the altered properties of every mutation in a single protein.

In a previous communication we described the expression of two mutants of c-actin causing HCM (p.Y166C and p.M305L) by the *Sf21/baculovirus* system and their purification in native state that subsequently allowed their biochemical and cell biological characterization [39]. In the current study we investigated the functional properties of further mutants of cardiac α-actin purified after recombinant expression as native and tag-free proteins with the aim to analyse the mechanisms, by which these mutants might induce the development of the HCM or DCM phenotype. Detailed knowledge of these processes is still lacking. The mutant p.A295S located in subdomain 3 has been reported to cause HCM with high penetrance [17] and was shown to perturb the interaction of actin filaments with tropomyosin [64]. The c-α-actin mutations p.R312H located in subdomain 4 and p.E361G in subdomain 1 (Fig. 1) are reported to cause DCM [2,11,55] with a benign outcome [11].

Here we compared wild-type cardiac actin with the listed mutants in a number of different assays. In summary, we observed subtle differences in the biochemical and cell biological properties of the isolated c-α-actin mutants In comparison to wt c-α-actin. Our data indicate that after purification the c-α-actin variants were in native state and able to polymerize albeit with different kinetics and form normally appearing filaments of varying lengths. Further detected altered properties concern the $Ca^{2+}$-sensitivity after decoration with tropomyosin (Tm) and troponin (Tn) complex or their interactions with other isolated sarcomeric and cytoskeletal proteins. These alterations might however have a larger impact when interacting with other regulatory proteins during cardiomyocyte development or within the intact sarcomere.

## Materials And Methods

# Materials

# Antibodies

Monoclonal mouse anti-skeletal α-actin (clone AC-1-20.4), anti-ß-actin (clone AC15), mouse anti-sarcomeric α-actinin, rabbit anti-all actins (clone C11) antibodies were obtained from Sigma-Aldrich (Munich, Germany). Donkey anti-mouse Alexa Fluor® 488 or 568 and anti-rabbit Alexa Fluor® 488 or 568 antibodies were from Molecular Probes (Eugene, Oregon; USA). Goat anti-HA (clone Y-11) antibody was obtained from Santa Cruz Biotechnology (Dallas, Texas, USA); mouse anti-cardiac α-actin was purchased from Progen Biotechnik GmbH (Heidelberg, Germany). Monoclonal anti-myomesin (clone B4) antibody (Grove et al., 1984) was a kind gift from Dr. E. Ehler (King's College London, London, U.K.).

## Clones:

The pcDNA3.1/NT-GFP-TOPO®-WT-α-cardiac actin and the mutants p.A295S, p.R312K, and p.E361G were donated from Dr. Cora-Ann Schoenenberger (University Basel, Switzerland). The p.R312H mutant was generated by site-directed mutagenesis from the p.R312K variant. Since the biochemical properties of the p.R312K variant were found to be very similar to wt c-actin, the results of its analysis are included in the Supplementary Information. The c-α-actin containing plasmids served as templates for cloning the c-α-actin variants into p3xHA-C1 plasmid. The p3xHA-C1 plasmid was a kind gift from Dr. T. Engel (Leibniz-Institut für Arteriosklerosis, Münster University, Germany), who deleted cDNA of EGFP from pEGFP-C1 plasmid (Clontech) and instead cloned into this plasmid the cDNA of a three times repeated hemagglutinin-tag (HA). The primers used for amplifying the actin cDNAs were as follows: 5'-GTTATGTGTGACGACGAGGAGACC-3' and 5'-ATTGCCCTTTTAGAAGCATTTGCG-3'. PCR inserts were cloned into p3xHA-C1 using *Xba*I and *Xho*I sites.

The deletion construct of human gelsolin G4-6 was kindly supplied by Dr. A.G. Weeds (MRC-LMB, Cambidge, UK) and subcloned from shuttle vector pKN172 into the cold-shock expression plasmid

pCOLD II (Takara Bio Inc., Kusatsu, Japan) using the restriction sites for *Bam*HI and *Hind*III enzymes obtained from Fermentas (Vilnius, Lithuania). The pCOLD II plasmid provides a His-Tag sequence for affinity chromatography, which was fused to the N-terminus of G4-6and subsequently used to affinity-purify the c-α-actins [39,42]. Arp2/3 complex isolated from *Acanthameba castellani* was kindly supplied by Prof. M. Barber (San Francisco, California, USA) and mDia3-FH2 by Prof. Alfred Wittinghofer (MPI, Dortmund, Germany).

# Reagents

Pyrene-maleinimide was obtained from Sigma Aldrich (Munich, Germany). All reagents were of analytical grade.

# Protein expression and purification

Rabbit skeletal muscle and bovine c-α-actin were prepared from dried acetone powder and human cardiac muscle wt α-actin and its mutants were expressed in the *baculovirus/Sf21*-system [2,39] as detailed in the Supplementary Information. Preprations of myosin subfragment 1 (myosin-S1) from skeletal muscle and bovine cardiac muscle [58], of cardiac tropomyosin (cTm) [4,21] and troponin complex (cTn) [1,10,12], the N-terminal C0C2 fragment of human cardiac MyBP-C [51], and the gelsolin deletion mutant G4-6 [42] were performed with modifications of published procedures as detailed in the Supplementary Information.

# Analytical procedures

## ATPase assay

Stimulation of the ATPase activity of ß-cardiac or skeletal muscle myosin-S1 activated by human wt cardiac α-actin or the cardiomyopathy inducing mutants was performed at 25 °C using a modified version of NADH-coupled assay according to [35] in a buffer containing 40 mM HEPES, pH 7.4, 25 mM KCl, 2 mM $MgCl_2$, 0.5 mM DTT, 0.2 mM NADH and an ATP regeneration system consisting of 0.05 mg/ml pyruvate kinase, 0.5 mM PEP, and 0.02 mg/ml LDH. The reaction was started by addition of myosin-S1 to a final concentration of 1 µM. NADH oxidation was followed by measuring the decrease in absorption at 340 nm ($\varepsilon$ = 6220 $M^1$ $cm^{-1}$) [48,61] using a spectrophotometer (DU 800, Beckman Coulter, Krefeld, Germany). The ATPase rates were determined by linear curve fitting and repeated at least three times for each condition with at least two different c-actin variant purifications.

## DNase I inhibition assay

The DNase I inhibition assay was performed as described [34]. The DNase test solution contained 50 µg/ml salmon sperm DNA (Sigma-Aldrich D1626) in 10 mM Tris-HCl, pH 8.0, 1 mM $MgCl_2$ and 0.1 mM $CaCl_2$. To determine the endonuclease activity of DNase I, a 10 µl pre-incubation reaction containing 3.2 µM DNase I from bovine pancreas (Sigma-Aldrich DN25) and zero to 6.4 µM of G-actin was prepared

in G-buffer and incubated at room temperature for 20 min. Aliquots of the samples were added to 0.8 ml of 50 µg/ml DNA-solution and the absorbance was immediately monitored at 260 nm for 10 min using the Beckman DU 800 spectrophotometer. From the ratio of the initial linear rates of DNase I activity were determined and expressed as Kunitz units (KU/min; 1 KU = ΔOD 260 nm of 0.001).

## Gel electrophoresis

Polyacrylamide gel electrophoresis in the presence of SDS (SDS-Page) was performed as given [30]. Native gel electrophoresis was performed on 10% polyacrylamide gels without SDS and run as described previously [47].

## Immunoblotting:

Cells were lysed 10 mM Tris-HCl, pH 7.4, 100 mM NaCl, 1 mM EDTA, 1 mM EGTA, 1 mM NaF, 20 mM $Na_4P_2O_7$, 2 mM $Na_3VO_4$, 1% Triton X-100, 10% glycerol, 0.1% SDS, 0.5% deoxycholate) and vortexed for 30 s and frozen until use. After thawing, the extracts were vortexed again and centrifuged at 20,817x g at 4 °C for 5 min. The protein concentration was estimated according to Bradford [7]. 30 µg of protein extracts were separated on 12.5 % SDS-Page gels. Proteins were transferred to nitrocellulose membrane using a wet blotter [24,59]. Subsequently the membranes were blocked for 1 h in Tris-buffered saline with 1% Tween-20 (TBS-T) containing 5 % non-fat milk powder (blocking solution) and then incubated overnight at 4 °C with primary antibody diluted in blocking solution (goat anti-HA 1:500, mouse anti-α-cardiac actin 1:200, mouse anti-α-actinin 1:2,000, mouse anti-GFP at 1:2,500 and rabbit anti-actin C11 at 1:1,000 dilution). After three washing steps with TBS-T for 15 min at room temperature, the nitrocellulose sheets were incubated with secondary antibodies linked to horse radish peroxidase (HRP) diluted in blocking solution (1:2,000) directed against either mouse or rabbit or goat for 1 h at RT. The nitrocellulose membranes were developed with the help of enhanced chemiluminescence (ECL) system (GE Amersham, Stepstone, UK). Occasionally membranes were subsequently stripped, re-blotted and immunostained for total actin.

## Actin polymerization assays:

Actin polymerization rates were determined by the increase in fluorescence caused by incorporation of pyrene-labelled actin into actin filaments [28,39]. Pyrene-labelled actin was pre-cleared by dialysis against G-buffer (10 mM Tris-HCl, pH 8.0, 0.2 mM $CaCl_2$, 7 mM β-mercaptoethanol, 1 mM ATP) and centrifugation at 100,000xg for 30 min. In these tests we used pyrene-labelled skeletal muscle actin that was added to the c-actins at a ratio of 20:1 (0.25 to 5 c-α-actin). Since pyrene-labelled skeletal-actin on its own at 0.25 µM did not show significant polymerization, i.e. increase in fluorescence. Therefore, we assume that the increase in fluorescence observed after mixing it with globular c-α-actin in G-buffer was solely due to the polymerization of the c-α-actins. Polymerization was induced by addition of 2 mM $MgCl_2$ and 0.1 M

KCl. Though The increase of pyrene fluorescence with excitation wavelength of 365 nm was monitored at 385 nm using a Schimadzu RF5001PC spectrofluorometer.

## Critical concentration

To determine the critical concentration of c-α-actin polymerization the varying concentrations of the c-α-actins supplemented with 5% pyrene-actin were polymerized in the presence of 2 mM $MgCl_2$ and 0.1 M KCl overnight. The actin concentrations varied from 0.1 to 10 µM. The steady-state fluorescence of polymerized actin was plotted versus monomeric actin concentration and the critical concentration was calculated form the intersections with the abscissa.

## Determination of the $Ca^{2+}$-dependence of Tm movement on cardiac F-actins:

The $Ca^{2+}$-dependence of pyrene-labelled cTm movement on polymerized c-actin variants was determined by the increase of the eximer pyrene-fluorescence at excitation and emission wavelengths of 340 nm and 480 nm, respectively, using an Infinite 200 microplate reader (Tecan, Männedorf, Switzerland). Thin filaments were reconstituted from each c-actin variant with pyrene-labelled cTm and reconstituted cTn complex, myosin-S1, and N-cMyBP-C each added at a 1:6 molar ratio to actin subunits. Distinct free $Ca^{2+}$-concentrations in the presence of 1 mM ATP were generated in black 96-well plates [10]. Fluorescence intensities were corrected for background fluorescence and normalized to $F_{max}$ = 1 and $F_{min}$ = 0. Nine experiments were performed for each c-α-actin variant and condition. The data were fitted using a normalized Hill equation (Sigma Plot, Systat Software, Erkrath, Germany).

# Generation of recombinant adenoviruses

For the generation of recombinant adenoviruses (Ad) the AdEasy™ kit (Qbiogene) was applied [37,39]. DNA sequences encoding wt- and the mutants A295S-, R312H-, and E361G- c-α-actins fused at the N-terminus to a HA-tag were amplified by PCR with the primers: 5'ATCATGGATTACCCATACGATGTTC-3' and 5'-ATCGCCCTTTTAGAAGCATTTGCG-3'. As templates served p3xHA-C1 plasmids encoding wt and the mutant cardiac α-actins. The *EcoR*V site was used to clone PCR inserts into pAdTrack-CMV shuttle plasmid. Electro-competent bacteria *E.coli* BJ5183 were simultaneously transformed with the shuttle plasmid linearized with the help of *Pme*I and adenoviral AdEasy-1 DNA backbone. Following homologous recombination in bacteria, clones were screened by restriction with the *Pac*I enzyme that in the case of positive clones resulted in two 33 kb and 4.5 kb fragments. Lipofectamine™ (Invitrogen) reagent was used to transfect HEK293 cells with linearized pAdEasy-1 construct encoding wild type and the mutant cardiac α-actins. Since pAdEasy-1 lacks of E1 and E3 genes critical for successful packaging of adenoviruses, it was crucial to generate adenoviral particles in HEK293 cells, which contain these two genes. The adenoviral DNA encoded additionally EGFP enabling tracking the generation of viral particles. After two to three weeks, the cells were lysed liberating viral particles. HEK293 cells were twice re-infected

with recombinant adenoviruses in order to obtain higher amounts of viral particles. For more details concerning the structure of recombinant adenoviral DNA and the steps of recombinant adenoviruses generation see [22]. The correctness of DNA constructs was verified by sequencing.

# Cell culture and immunohistological procedures

## Cells

HeLa, C2C12 were from DSMZ (Deutsche Sammlung von Mikroorganismen und Zellkulturen, Braunschweig, Germany) and MDCK cells (Marvin-Darby canine cells) were kindly supplied by Prof. Anna Starzinski-Powitz (Frankfurt, Germany). The cells were propagated in DMEM medium containing 0.5% glucose, 1% penicillin/streptomycin, 1% glutamine, 0.5% sodium pyruvate, and 10% fetal calf serum. Cells were cultured in 25 $cm^2$ flasks (Falcon®, Becton Dickinson GmbH, Heidelberg, Germany) at 37 °C in 5% $CO_2$ and 90% humidified air and split weekly, using 0.25% trypsin/0.05% EDTA solution.

Cardiomyocytes from 1–5 days old rats were isolated following the modified protocol described in [16,37] as detailed in the Supplementary Information.

## Cell transfection

The cells were seeded on glass coverslips in 6-well plates (3 x $10^5$ cells/well) and transfected with the help of MATra-A reagent (Iba, Munich, Germany) with 3 µg of DNA encoding either for GFP-actins or HA-actins. For Western blot analysis the cells were seeded in 6 cm plastic Petri dishes and transfected with 5 µg DNA. 24 h or 48 h after transfection the cells on coverslips were fixed with 4% formaldehyde (FA) or harvested in Petri dishes in lysis buffer using a rubber policeman.

NRCs were infected with 20 µl of adenoviruses added to 2 ml of medium following the procedure described [39]. 72 h after infection the cells were either fixed with warm (37 °C) 4% formaldehyde (FA) for immunocytochemistry or harvested with the help of rubber policeman for Western blotting. For controls, cells were infected with only EGFP-encoding viruses.

## Confocal microscopy

Control cells, transfected cells and those infected with adenoviruses were fixed with warm (37 °C) 4% FA for 20 min at RT and permeabilized with 0.1% Triton X-100 in PBS for 6 min. For staining with anti-cardiac α-actin-antibody, we additionally fixed the cells with ice-cold methanol for 6 min at 4 °C. After fixation the coverslips or plastic dishes were blocked for 30 min with 3% BSA in PBS. All antibodies were diluted in PBS containing 3% BSA. The cells were immunostained either with goat anti-HA IgGs, or with monoclonal antibodies directed against anti-β-actin, anti-c-α-actin, anti-sarcomeric α-actinin, and anti-myomesin. The secondary IgGs were conjugated either with Alexa Fluor® 488 or Alexa Fluor® 568. In the case of double immunostaining, when the goat anti-HA antibody was applied, donkey anti-mouse IgGs were used in

order to avoid cross-reactivity. F-actin was visualized by staining with TRITC-conjugated phalloidin (Sigma-Aldrich). The nuclei were visualized with the help of Hoechst 33342 (Riedel-de-Haen). The coverslips or plastic dishes were washed several times with PBS for 5 min. After all incubations and washing steps the cells were mounted in DAKO cytomatic fluorescent mounting medium. Immunofluorescence microscopy was performed using a Zeiss LSM 800 laser-scanning microscope (Jena, Germany). For documentation at least 5 cells were photographed from three independent experiments and a representative image is presented. Co-localization analysis was performed by using ZEN 2007 software (Carl Zeiss Vision GmbH, Goettingen, Germany) and confirmed when the Pearson's correlation coefficient was > 0.3.

Control cells, transfected cells and those infected with adenoviruses were fixed with warm (37 °C) 4% FA for 20 min at RT and permeabilized with 0.1% Triton X-100 in PBS for 6 min. For staining with anti-cardiac α-actin-antibody, we additionally fixed the cells with ice-cold methanol for 6 min at 4 °C. After fixation the coverslips or plastic dishes were blocked for 30 min with 3% BSA in PBS. All antibodies were diluted in PBS containing 3% BSA. The cells were immunostained either with goat anti-HA IgGs, or with monoclonal antibodies directed against anti-β-actin, anti-c-α-actin, anti-sarcomeric α-actinin, and anti-myomesin. The secondary IgGs were conjugated either with Alexa Fluor® 488 or Alexa Fluor® 568. In the case of double immunostaining, when the goat anti-HA antibody was applied, donkey anti-mouse IgGs were used in order to avoid cross-reactivity. F-actin was visualized by staining with TRITC-conjugated phalloidin (Sigma-Aldrich). The nuclei were visualized with the help of Hoechst 33342 (Riedel-de-Haen). The coverslips or plastic dishes were washed several times with PBS for 5 min. After all incubations and washing steps the cells were mounted in DAKO cytomatic fluorescent mounting medium. Immunofluorescence microscopy was performed using a Zeiss LSM 800 laser-scanning microscope (Jena, Germany). For documentation at least 5 cells were photographed from three independent experiments and a representative image is presented. Co-localization analysis was performed by using ZEN 2007 software (Carl Zeiss Vision GmbH, Goettingen, Germany) and confirmed when the Pearson's correlation coefficient was > 0.3.

Control cells, transfected cells and those infected with adenoviruses were fixed with warm (37 °C) 4% FA for 20 min at RT and permeabilized with 0.1% Triton X-100 in PBS for 6 min. For staining with anti-cardiac α-actin-antibody, we additionally fixed the cells with ice-cold methanol for 6 min at 4 °C. After fixation the coverslips or plastic dishes were blocked for 30 min with 3% BSA in PBS. All antibodies were diluted in PBS containing 3% BSA. The cells were immunostained either with goat anti-HA IgGs, or with monoclonal antibodies directed against anti-β-actin, anti-c-α-actin, anti-sarcomeric α-actinin, and anti-myomesin. The secondary IgGs were conjugated either with Alexa Fluor® 488 or Alexa Fluor® 568. In the case of double immunostaining, when the goat anti-HA antibody was applied, donkey anti-mouse IgGs were used in order to avoid cross-reactivity. F-actin was visualized by staining with TRITC-conjugated phalloidin (Sigma-Aldrich). The nuclei were visualized with the help of Hoechst 33342 (Riedel-de-Haen). The coverslips or plastic dishes were washed several times with PBS for 5 min. After all incubations and washing steps the cells were mounted in DAKO cytomatic fluorescent mounting medium. Immunofluorescence microscopy was performed using a Zeiss LSM 800 laser-scanning microscope

(Jena, Germany). For documentation at least 5 cells were photographed from three independent experiments and a representative image is presented. Co-localization analysis was performed by using ZEN 2007 software (Carl Zeiss Vision GmbH, Goettingen, Germany) and confirmed when the Pearson's correlation coefficient was > 0.3.

# Electron microscopy

For negative staining F-actin samples were diluted to 0.1 mg/ml and adsorbed to freshly glow-discharged carbon-coated copper grids (200 mesh) for 45 sec. Negative staining with 1.0% uranyl acetate was performed as described [26,48]. The samples were examined in a Zeiss electron microscope EM923 (SESAM) run at 150 kV fitted with a TemCamF416 camera (Tietz Video and Image Processing Systems, Gauting, Germany).

# Data evaluation

DNA sequences were analysed in DNAstar Lasergene software (DNASTAR Inc., Madison, Wisconsin, USA). Densitometric analysis of bands was performed with the help of the Ultra Quant 6.0 software (Thermo Fisher Scientific, Schwerte, Germany). Graphs were plotted in Excel 2007 (Microsoft®) or in Origin 8.5 (OriginLab). In both the myosin-S1 ATPase activity and $Ca^{2+}$-dependence of cTm movement assays the data are given as mean values (± SEM, standard error of the mean). In addition, the significance of the $Ca^{2+}$-dependency data were analysed by the Student´s t-test and the R-square ($R^2$) analysis using Sigma Plot Software (Systat, Erkrath, Germany).

## Results

# Expression and purification of the cardiac α-actin variants

Expression of the c-α-actins (wt plus the mutants) was achieved in *Sf21* insect cells by using the *baculovirus* system and purified after affinity binding to gelsolin G4-6 as reported previously [39] (shown for wt and the p.E361G mutant in the Online Supplementary Information; Fig. S1A,B). The isolated proteins showed only one main band after SDS-Page (Fig. 2A) and were shown to be cardiac α-actin by immunoblotting using an anti-cardiac α-actin antibody (dot blots Fig. 2B and Western blots in Fig. 2C). Since it was suspected that this purification procedure does not discriminate between the expressed cardiac and endogenous insect cell actin, we performed also immunoblots with an anti-ß-actin antibody [37,39] assuming that this antibody recognized the endogenous actin of the insect *Sf21*-cells. Indeed, after expression in *Sf21*-cells the purified cardiac actins possessed ß-actin immune-reactivity (Fig. 2C). Cardiac α-actin was also conventionally purified from acetone powder obtained from bovine hearts. After SDS-Page its migration behaviour and reactivity in Western blots against anti-cardiac α-actin was found identical to recombinant wt c-α-actin. In contrast, prominent anti-β-actin reactivity was observed for purified bovine c-α-actin (Fig. 2C) probably due to the presence of β-actin in either fibroblastic cells or sub-membranously within the cardiomyocytes themselves.

Initially we had aimed to selectively extract the expressed cardiac α-actins using a N-terminal His-tag. This procedure, however, led to a considerable lower expression and furthermore the purified cardiac α-actins were suspected not to adopt a fully native configuration as they failed to polymerize. We generated also c-α-actin constructs containing a C-terminal thymosin β4-His-tag [6], however, in our hands also this approach led to only reduced expression and only small amounts could be purified that showed also reduced polymerizability. It was because of these failures that we switched to the previously used procedure using His-tagged gelsolin G4-6 as means to effectively affinity purify the *Sf21*-cell expressed cardiac actins.

# Tests for native configuration of the cardiac actin variants

After their purification the native state of the α-actins was verified by their ability to inhibit DNase I. All the purified c-α-actin variants inhibited deoxyribonuclease I (DNase I) activity. Wt c-α-actin inhibited with a lower efficiency than skeletal muscle actin (Fig. 3A). The p.R312H mutant inhibited with a similar activity as wt c-α-actin, whereas the p.E361G and the p.A295S mutants showed a higher or lower inhibitory capacity, respectively (Fig. 3A). These results suggested that the c-α-actin mutants might have attained slightly different conformations though none of the mutations is located within the DNase I-binding loop located in subdomain 2 [27]. Native gel electrophoresis used as additional test for their native conformation confirmed that all c-α-actin variants were able to bind thymosin β4 and gelsolin-segment 1 (G1) as described previously for other c-α-actin mutants (not shown; [39]).

# Polymerization behaviour of recombinant c-actins

The ability of the isolated cardiac actins to polymerize was analysed by measuring the fluorescence increase of added pyrenyl-actin [28]. Conventionally purified bovine cardiac actin showed almost identical polymerization behaviour as expressed wt c-α-actin (Fig. 3B) giving additional confirmation that the expression of c-α-actins by the *baculovirus/Sf21* system did not cause an impairment of its functionality. Clear differences, however, were observed between the mutant c-α-actin variants. The p.E361G DCM mutant showed the fastest polymerization kinetics (Figure 3F). Wt c-α-actin and the p.A295S (HCM) mutant polymerized with almost identical speed, whereas the DCM p.R312H mutant showed reduced kinetics and extent of polymerization (Fig. 3E) as also verified by the calculation of the half times of their polymerization (Table 1A). The critical concentrations of their polymerization (Cc) were determined separately (see Table 1B). The data obtained indicated that the Ccs did not differ significantly between wt c-α-actin and the mutants except the p.R312H mutant, which exhibited a higher Cc (Table 1) in agreement with previous data showing a higher thermal instability [67]. Table 1 contains also the data obtained for the p.R312K variant, which has been supposed to cause also DCM (personal communication (Dr. Schoenenberger, Basel, Switzerland). Since no clinical reports exist demonstrating a correlation of p.R312K to CM and its polymerization properties closely resembled wt c-α-actin (see Supplementary Information), we did include this variant in further studies.

Table 1
Polymerization parameters c-actins.

(A) Half times of polymerization determined in 5 independent experiments (see also Fig. 3B-F) in minutes

| Half time of polymerization ($t_{1/2}$) in min. | | | | | | |
|---|---|---|---|---|---|---|
| Bovine | c-actin | recomb. wt c-actin | p.A295S | p.R312H | p.R312K | p.E361G |
| 6.7 ± 0.6 | | 6.8 ± 0.3 | 5.5 ± 0.6 | 10.8 ± 0.9 | 2.5 ± 0.2 | 1.6 ± 0.2 |

Table 1
Polymerization parameters c-actins.

(B) independently determined critical concentrations of polymerization (Cc) of the cardiac actin variants (determined as detailed in Materials and methods). The experiments were repeated three times with two different protein preparations. Variations are given as SEM.

| Critical concentration of polymerization (Cc) in µM | | | | | | |
|---|---|---|---|---|---|---|
| Bovine | c-actin | recomb. wt c-actin | p.A295S | p.R312H | p.R312K | p.E361G |
| 0.21 ± 0.1 | | 0.2 ± 0.09 | 0.4. ± 0.3 | 0.7 ± 0.12 | 0.21 ± 0.12 | 0.2 ± 0.11 |

# Polymerization behaviour of recombinant c-α-actins in the presence of nucleators

During cardiomyocyte differentiation and sarcomerogenesis a number of different actin-binding proteins are involved in the processes of microfilament transformation into sarcomeres [8]. Indeed recent data have shown the presence of actin polymerization nucleating factors (nucleators) in cardiac muscle [52]. Therefore, we analysed the polymerization behaviour of the c-α-actin variants in the presence of the nucleators Arp2/3 complex and the active FH2-domain of the formin mDia3, which induce either actin filament networks or straight filaments, respectively [29]. In these experiments the nucleators were added to actin at a 100:1 ratio before initiating polymerization. The data showed that both nucleators stimulated the polymerization rate of wt c-α-actin (Fig. 3D), whereas the polymerization of the mutants was affected differently: The HCM p.A295S mutant was clearly stimulated by mDia3-FH2, but only minimally by Arp2/3 complex (Fig. 3E). In contrast, the DCM mutant p.R312H was stimulated by both nucleators albeit more strongly by mDia3-FH2 (Fig. 3G). In contrast, Arp2/3 complex had only a small stimulating effect on the rate of polymerization of the p.E316G mutant, whereas mDia3-FH2 appeared not to affect its polymerization behaviour (Fig. 3H). The data (compiled in Table 2) show that the polymerization of most c-α-actin variants was stimulated by mDia3-FH2, except the p.E316G mutant. In summary, these data show significant differences in the polymerization behaviour of the analysed c-α-

actin variants and its modulation by these nucleating actin-binding proteins that might have functional consequences during cardiomyocyte development.

Table 2
Effect of polymerisation nucleators on cardiac actin variants. Polymerisation parameters of 5 µM cardiac actin variants in the absence or presence of 50 nM Arp2/3 complex or 50 nM mDia3-FH2 (data taken from Fig. 3D-G). The experiments were repeated three times with two different protein preparations.

| Half times of polymerization ($t_{1/2}$) in minutes in the presence of nucleators (data taken from Fig. 3D-G). | | | | |
|---|---|---|---|---|
| | recomb. wt c-actin | p.A295S | p.R312H | p.E361G |
| control | 8.6 | 12.2 | 13.8 | 4.0 |
| Arp2/3 complex | 2.1 | 1.2 | 1.0 | 1.8 |
| mDia3-$FH_2$ | 6.9 | 3.5 | 4.1 | 2.9 |

# Electron microscopy of filaments formed by the c-actin variants

Filament formation was further verified by electron microscopy after negative staining (EM) before and after decoration with cardiac tropomyosin (cTm) and troponin complex (cTn) at molar ratio of 7:1:1 (Fig. 4). The data indicated formation of normally appearing actin filaments at this resolution for bovine and wt recombinant c-α-actin (Fig. 4C). Decoration of with cTm and cTn led to straighter and apparently longer filaments (Fig. 4). EM showed that the mutants p.A295S and p.R312H formed more curved filaments and frequently exhibited strand breaks (Fig. 4D,E). The p.E361G mutant formed curved and often only short filaments (Fig. 4F). After decoration with cTm/cTn, all mutants formed more regular and longer filaments though the p.R312H mutant appeared to retain the wavy appearance and fragmentations were still occasionally detectable (Fig. 4E´).

# $Ca^{2+}$-dependence of the myosin-S1 ATPase stimulation by c-α-actin variants

The main function of filamentous actin is the stimulation of the myosin ATPase activity during its cyclic interaction with myosin-heads leading to muscle contraction. Therefore we determined the stimulation of the myosin-S1 ATPase by the c-actin variants under two different conditions. The c-actin concentration dependency is given in the Supplementary Information and showed that decoration of the c-actin variants

with cTm and cTn increased their stimulatory activity except for the p.R312H mutant (Fig. S3 and Table S1).

Next we determined the $Ca^{2+}$-concentration dependence of the myosin-S1 ATPase stimulation after decoration of the filamentous c-actins with cTm/cTn (see Materials and methods). The absolute ATPase rates (shown in Figure 5A,B and D-F) indicate a rather similar extent of stimulation albeit the maximal ATPase stimulation was highest for bovine c-α-actin and p.A295S (Table 3). The superposition of the normalized rates indicate that bovine and recombinant wt c-α-actin stimulate the myosin-S1 ATPase with a similar $Ca^{2+}$-dependence (Fig. 5C and Table 3). The superposition of the $Ca^{2+}$-dependences of the stimulation of the myosin-S1 ATPase by wt and the three c-α-actin mutants shown in Figure 5G indicated that in comparison to wt c-α-actin the p.A295S mutant showed a slightly higher and the two DCM mutants (p.R312H and p.E361G) a rather similar $Ca^{2+}$-sensitivity (Fig. 6G). The $pCa_{50}$ values and differences in Hill coefficients are compiled in Table 3.

Table 3

Parameters from Ca2+ -ion dependence of myosin-S1 ATPase stimulation. Parameters are derived from experiments depicted in Figure 5. All measurements were performedfor each c-actin variant in filamentous form after decortion with cTm and cTn at a ratio of 6:1:1. Hill coefficients, pCa50-values and the R-squared (R2) values were calculated by the Sigma Plot Systat Software (Erkrath, Germany). N gives the number of experiments. Variations are given as SEM. The fold stimulation was calculated from the ratio of the maximal (max.)/minimal (min.) ATPase activity.

| actin variant | $pCa_{50}$ | Hill coefficient | min. ATPase<br>µM ATP hyd/µM S1/s | max. ATPase<br>µM ATP hyd/ µMS1/s | fold stimulation (pCa max./min.) |
|---|---|---|---|---|---|
| Bovine N = 3 $R^2$ = 0.891 | 6.933 ± 0.204 | 1.182 ± 0.54 | 0.086 | 0.44 | 5.625 |
| WT rec N = 4 $R^2$ = 0.894 | 6.844 ± 0.093 | 1.68 ± 0.559 | 0.093 | 0.379 | 4.0 |
| p.A295S N = 3 $R^2$ = 0.933 | 7.060 ± 0.097 | 1.497± 0.452 | 0.078 | 0.387 | 4.96 |
| p.R312H N = 3 $R^2$= 0.789 | 6.923 ± 0.196 | 1.342 ± 0.824 | 0.054 | 0.346 | 5.83 |
| p.E361G N = 3 $R^2$ = 0.927 | 6.844 ± 0.116 | 1.021 ± 0.256 | 0.057 | 0.301 | 5.0 |

The data additionally show that the HCM p.A295S mutant possesses in comparison to cTm/cTn decorated wt c-α-actin and the two DCM mutants a higher $Ca^{2+}$-sensitivity (p.R312H and p.E361G), but a lower Hill coefficient (Table 3), i.e. cooperative propagation ability of the myosin-S1 binding (Table 3). The reduced Hill coefficient of the DCM mutants might be due to the fact that the p.R312H and p.E361G mutations are located within the cTm and the myosin head binding regions, respectively (see also Discussion).

Student t-distribution tests and R square ($R^2$) analysis indicated that the measurements were significant for each special condition albeit not of high significance when comparing different mutants with each other or different conditions (varying compositions of actin-binding proteins, see also Table 3).

# $Ca^{2+}$-dependence of tropomyosin movement on c-α-actin variants

Binding of one $Ca^{2+}$-ion to the cardiac troponin subunit TnC induces a conformational alteration of the Tn complex leading to an azimuthal movement of Tm along the actin filament and the exposure of binding sites for myosin heads [13]. Functionally three different Tm positions have been identified: (i) in relaxed muscle the blocked (B-) state, that inhibits myosin head attachment, (ii) upon cytosolic $Ca^{2+}$-ion increase and binding to TnC the Tm moves to the closed (C-) state, that allows binding of myosin heads with low affinity, (iii) and finally induced by myosin head binding the open (M-) state allowing their binding with high affinity [5,19,20,32,62]. The extent of Tm movement is largest (azimuthal angle of about 20°) when going from the B- to the C-state, whereas the transition to the M-state requires only a smaller azimuthal movement (angle change about 5°). Due to a lower energy barrier the transition from C- to M-state occurs much more readily in cardiac than skeletal muscle [32].

Cardiac Tm is a homodimer composed of two α-chains. Labelling with pyrenyl- maleinimide occurs at Cys190 of both chains producing a fluorescent eximer [21] that allows to monitor the $Ca^{2+}$-dependency of cTm movement on F-actin from the closed (C-) to the open (M-) state [25]. Using this assay we analysed whether the observed $Ca^{2+}$-sensitivities of the ATPase stimulation were paralleled by a similar behaviour of the Tm movement, i.e., a fluorescence increase of pyrene-cTm. Therefore, polymerized c-α-actins were decorated with pyrene-labelled cTm and cTn at a 6:1:1 molar ratio (see Materials and methods). Due to the low energy barrier of the C- to M-state transition of cardiac muscle, we expected to observe only a single step in fluorescence increase of pyrene-cTm.

The measurements were performed for four different conditions: in the absence and presence of cardiac myosin-S1 plus 1 mM ATP and for both cases with the additional presence of the F-actin binding N-terminal fragment of cardiac myosin binding protein C comprising the C0, C1, M, and C2 domains (subsequently named N-cMyBP-C; for details see Discussion). The C1-domain has been shown to bind to subdomain 1 of actin and cTm, thereby increasing the $Ca^{2+}$-sensitivity of native cardiac thin filaments [43,51,57]. In native muscle the M-domain is phosphorylated in response to external signals, however, in

our experiments we used recombinantly expressed and therefore non-phosphorylated N-cMyPB-C. Like cTm and cTn cardiac N-MyBP-C and cardiac myosin-S1 (where indicated) were added at a 6fold lower molar concentration to actin subunits.

In a first series of experiments we compared recombinant wt with conventionally purified bovine c-α-actin (Fig. 6). Surprisingly, the $Ca^{2+}$-sensitivity of the cTm movement in the presence of only cTm/cTn was lower than that of the stimulation of the myosin-S1 ATPase (Fig. 6; compare Table 3 and 4). The data, however, showed that the addition of myosin-S1 did not increase the $Ca^{2+}$-sensitivity of bovine but of the c-α-actins (Fig. 6; Table 4). However, in the presence of myosin-S1 both bovine and wt c-α-actin exhibited almost identical $Ca^{2+}$-dependency of cTm movement (Fig. 6). Addition of N-cMyBP-C, however, resulted in an increase in $Ca^{2+}$-sensitivity of both bovine and recombinant wt c-α-actin in the absence and presence myosin-S1 (Fig. 6; Table 4). These data indicate that also under conditions more closely resembling the natural situation both bovine and recombinant c-α-actin behaved identically.

Next we tested the $Ca^{2+}$-sensitivity of the mutant c-α-actins after decoration with cTm and cTn under identical conditions. The p.A295S mutant (correlated with HCM) showed an increased $Ca^{2+}$-sensitivity when compared to the p.R312H and p.E361G mutants (correlated to DCM). All mutants showed a decreased $Ca^{2+}$-sensitivity when compared to wt c-α-actin. Differences were observed between the mutant c-α-actins in their $Ca^{2+}$-sensitivity and the effects of addition of myosin-S1 and N-cMyBP-C (Fig. 6; Table 4). In the presence of myosin-S1 the p.A295S mutant showed the highest $Ca^{2+}$-sensitivity in comparison to wt and both DCM mutants (Fig. 6E, Table 4). Addition of N-cMyBP-C had a slightly "flatting" effect on the $Ca^{2+}$-sensitivity, i.e. a decrease of the Hill coefficient from 1.7 to 0.98 (Table 4).

Table 4

Parameters of the Ca2+-ion dependence of fluorescence increase of pyrene-cTm; i.e. cTm movement The c-actin variants were decorated with pyrene-labelled cTm at a ratio of 6:1 and the dependence of the increase of pyrene-fluorescence on Ca2+-concentration was determined (see Materials and methods) in the absence or additional presence of myosin-S1 alone and/or plus N-cMyBP-C. Hill coefficients, pCa50-values and the R2-coefficient were calculated by the Sigma Plot Systat Software (Erkrath, Germany). N gives the number of experiments. Variations are given as SEM.

| | bovine c-actin | | recomb. wt c-actin | |
|---|---|---|---|---|
| | $pCa_{50}$ | Hill | $pCa_{50}$ | Hill |
| + cTm/cTn | 7.327 ± 0.147 (N = 9; $R^2$ = 0.724) | 1.032 ± 0.27 | 7.555 ± 0.215 (N = 4; $R^2$ = 0.797) | 0.888 ± 0.317 |
| + S1 | 7.53 ± 0.128 (N = 6; $R^2$ = 0.8128) | 1.224 ± 0.31 | 7.45 ± 0 .13 (N = 4; $R^2$ = 0,8713) | 1.31 ± 0.36 |
| + N-cMyBP-C | 7.15 ± 0.14 (N = 2; $R^2$ = 0.901) | 1.52 ± 0.67 | 7.48 ± 0.17 (N = 3; $R^2$ = 0.913) | 1.74 ± 0.63 |
| + S1 + N-cMyBP-C | 7.47 ± 0.2 (N = 3; $R^2$ = 0.789) | 1.1 ± 0.42 | 7.32 ± 0.06 (N = 3; $R^2$ = 0.977) | 1.58 ± 0.26 |

| | p.A295S | | p.R312H | | p.E361G | |
|---|---|---|---|---|---|---|
| | $pCa_{50}$ | Hill | $pCa_{50}$ | Hill | $pCa_{50}$ | Hill |
| + cTm/cTn | 7.32 ± 0.1 (N = 9; $R^2$ = 0.873) | 1.55 ± 0.43 | 7.1 ± 0.03 (N = 3; $R^2$ = 0.950) | 3.9 ± 2.4 | 7.6 ± 0.11 (N = 6; $R^2$ = 0.90) | 1.05 ± 0.2 |
| + S1 | 7.26 ± 0.61 (N = 4; $R^2$ = 0,8638) | 1.74 ± 0.61 | 6.76 ± 0.21 (N = 5; $R^2$ = 0.817) | 1.28 ± 0.26 | 7.07 ± 0.07 (N = 6; $R^2$ =0.7614) | 2.77 ± 1.56 |
| +N-cMyBP-C | 7.37 ± 0.1 (N = 5; $R^2$ = 0.936) | 0.85 ± 0.13 | 7.1 ± 0.09 (N = 3; $R^2$ = 0.936 | 1.42 ± 0.37 | 7.38 ± 0.2 (N = 3; $R^2$ = 0.879) | 0.86 ± 0.27 |
| +S1 + N-cMyBP-C | 7.22 ± 0.16 (N = 5; $R^2$ =0.842) | 0.96 ± 0.25 | 7.5 ± 0.17 (N = 3; $R^2$ = 0.893) | 1.69 ± 0.65 | 7.13 ± 0.14 (N = 3; $R^2$ = 0.878 | 1.33 ± 0.49 |

The p.R312H mutant showed a different behaviour. In the absence of myosin-S1 and N-cMyBP-C this mutant showed the steepest increase $Ca^{2+}$-sensitivity, i.e. the highest Hill coefficient (Table 4), which was reduced by about 50% after addition of myosin-S1 and/or N-cMyBP-C. Its $Ca^{2+}$-sensitivity was not affected by N-cMyBP-C, but further decreased by myosin-S1 (Fig. 6E).

In contrast, for the p.E361G mutant we observed in the absence of myosin-S1 and N-cMyBP-C the highest $Ca^{2+}$-sensitivity that was, however, reduced after addition of myosin-S1 and/or N-cMyBP-C (Fig. 6; Table 4).

Student-t test distribution and R-square ($R^2$) analysis indicated that the measurements were significant for each special condition albeit not of high significance when comparing different mutants with each other (see Table 3 and 4, which gives the $R^2$-values for each condition). Nevertheless, the data suggested that in the presence of only myosin-S1 the HCM p.A295S mutant showed a higher and the DCM R312H

and E361G mutants a lower $Ca^{2+}$-sensitivity than wt c-actin corresponding to a higher and lower contractility supposedly typical for HCM and DCM, respectively.

# Transfection of established cell lines with cardiac actin variants

The physiological or cell biological effects of these cardiac actin variants were tested also by transfection experiments into established cell lines like HeLa, C2C12 (not shown) and MDCK cells (Fig. 7). For the immunohistochemical localisation the c-α-actins were N-terminally tagged with a HA- (hemagglutinin) extension by standard procedures (see Materials and methods). After transfection (see Materials and methods), the cells were fixed, immunostained with anti-HA, TRITC-phalloidin and Hoechst 33342, and examined by confocal microscopy. The results obtained indicated that all c-α-actin variants incorporated into the cellular cytoskeleton of the three cell lines. The data collected for the MDCK cells are shown in Figure 7A-D and demonstrate that wt and p.A295S (HCM) mutant c-α-actins are preferentially incorporated into stress fibres forming either filamentous structures composed of apparently only the transfected c-α-actins as indicated by anti-HA staining (green; arrow in Fig. 7A,C) or copolymerizing with the endogenous actin (yellow arrow heads) in the merged images (Fig. 7A´´). In contrast, the p.R312H and p.E361G mutants did not significantly form stress fibres, but appeared to incorporate into apical structures of the polarized MDCK cells like the sub-membranous actin belt underneath presumed junctional contacts (arrows; Fig. 7B,D) and microvillar extensions (arrows in Fig. 7C,D).

# Infection of rat neonatal cardiomyocytes with the cardiac actin variants

In order to observe specific effects of the cardiac α-actin variants in their natural cell type, adenoviral constructs of the c-α-actin variants were generated as described [37,39] (see also Materials and methods) and used to transduce neonatal rat cardiomyocytes (NRCs) isolated from one to three days old newborn rats. For these experiments the c-α-actins were N-terminally HA-tagged for selective immunostaining. Subsequent TRITC-phalloidin staining allowed to observe their incorporation into the intracellular filament system, in particular into nascent sarcomeres (Figure 7E-I). The data indicate that the exogenous c-α-actins preferentially incorporated into or formed centrally located (around the nuclei) filamentous structures, whereas the TRITC-phalloidin staining appeared to be concentrated in peripheral filaments (Fig. 7E-I). Higher magnification of NRCs transfected with wt HA-c-α-actin showed a gradual increase in the concentration of the exogenous c-α-actins towards the cell centre (Fig. 7E), whereas the TRITC-phalloidin staining became weaker towards the cell centre (Fig. 7E) as indicated by a shift in the staining colour from yellow (overlap region) to green (Fig. 7E´). Sarcomeric structures were apparent in the periphery and within the yellow overlap region, whereas they appeared to vanish in the perinuclear region at the cell centre (Fig. 7E) suggesting that the transfected c-α-actin were generated within the perinuclear region and initially formed microfilaments before being transformed into sarcomeric structures.

Only the p.R312H mutant showed an additional peripheral localisation when HA-tagged (Fig. 7G). The fact that the centrally located filamentous c-α-actins were only weakly stained by TRITC-phalloidin may suggest that the HA-tag of the exogenous c- α-actins impaired its binding.

Since the N-terminal HA-tag blocks also the binding of the monoclonal anti-cardiac α-actin antibody [39], it became possible to differentiate by immunostaining the localisation of endogenous and exogenous c-α-actins. Indeed the obtained data supported the assumption of a distinct distribution of endogenous and exogenous c-α-actins in infected NRCs. Figure 8 shows a clear concentration of the anti-c-α-actin mAB immunostaining for endogenous actin (red; Fig. 8A and merge A´´) at the cell periphery or in peripheral extensions of NRCs expressing wt HA-c-α-actin (anti-HA immunostained in green; Fig. 8A). Similar results were obtained for NRCs infected with the p.A295S mutant (Fig. 8B; only merged image), the p.R312H mutant (Fig. 8C), or the p.E361G mutant (Fig. 8D). In NRCs transduced with vectors coding for the p.A295S or p.E361G mutant, the endogenous c-α-actin was concentrated in peripheral extensions but also present underneath the plasma membrane along the whole cell periphery where it appeared to partially co-localise with the exogenous mutant α-actins (Fig. 8B,D). Nevertheless, the exogenous c-α-actins were clearly concentrated in the middle of the infected NRCs.

Finally, transduced NRCs were counterstained with anti-α-actinin or -myomesin to identify the site of incorporation of the exogenous c-α-actins. Three days after isolation the NRCs had formed intracellular sarcomeric structures, which in some instances spanned the whole cytoplasm. Immunostaining with anti-α-actinin (Fig. 8E-I) or -myomesin (Fig. 8J-M) identified the Z- or M-lines, to which the thin filaments are attached by their plus ends or mark the minus ends, respectively. The data indicated that wt, p.A295S and p.R312H incorporated preferentially at the plus ends, i.e. at the region of the Z-lines (co-localisation with anti-α-actinin staining in Fig. 8E´,F,G), whereas the p.E361G c-actin did not colocalize with the anti-α-actinin staining (Fig. 8I). Only occasionally was a colocalisation of the p.E361G staining with anti-α-actinin detected (see below). The anti-myomesin staining revealed that wt, p.A295S and p.R312H did not colocalize with myomesin (Fig. 8I,K,L), but a significant colocalisation of p-E361G with the anti-myomesin staining (Fig. 8M). Figure 8M also indicated the additional presence of a faint anti-HA-band between the stronger anti-myomesin band colocalising with the anti-HA-p.E361G staining (arrow heads in Fig. 8M) indicating that a small fraction of HA-p.E61G had incorporated at the region of the Z-line. The preferential incorporation of the p.E361G actin at the minus end might be due to the fact that the mutated site is within the binding region of α-actinin, a Z-line component. These data suggest that in case of a high expression level of the p.E361G mutant the thin filament attachment to Z-line might be weakened leading to a reduced stability of the sarcomere.

# Discussion

Hypertrophic and dilative cardiomyopathies (CM) are the most frequent genetic diseases of the heart and caused to a high percentage by point mutations of genes encoding sarcomeric proteins. Here we analysed the biochemical and physiological properties of three mutations of cardiac α-actin correlated to cardiomyopathies. For this study wild type cardiac α-actin, the p.A295S mutant causing HCM, and the

p.R312H and p.E361G mutants correlated to DCM were expressed using the *Sf21/baculovirus* system, isolated in native state and analysed. It was hoped that analysing actin mutants causative for either of these two CM forms might reveal distinctly different properties that could be specifically attributed to a particular CM disease phenotype.

After purification the cardiac α-actins were pure as judged by SDS-Page, but appeared to contain about 10% cytoplasmic ß-actin as revealed by Western blotting with an anti-ß-actin specific antibody. We assumed that the source of ß-actin was the *Sf21* insect cells. Bovine cardiac α-actin purified from acetone powder contained about the same amount of ß-actin presumably present underneath the cardiomyocyte sarcolemma or in vessel walls. Unfortunately it was not possible to purify the c-α-actins after N-terminal tagging. Nevertheless, we are confident that the properties and activities of the purified α-actins are attributable to the cardiac α-actins, since the observed deviations from the wild type behaviour can only be due to alterations of the properties of the mutant forms.

The purified c-α-actins appeared to be in native state as verified by their ability to inhibit DNase I activity. Bovine, wt and the p.E361G mutant c-α-actin showed identical polymerization behaviour, whereas both p.A295S and p.R312H mutants polymerized much slower though the critical concentrations of polymerization (Cc) were similar and showed only a small difference from the Cc of bovine c-α-actin. Electron microscopy indicated that all α-actin variants formed typical filaments. The mutants, however, appeared to show filament breaks that became less frequent after decoration with cTm and cTn, a treatment that also led to more and longer filaments.

In muscle the function of F-actin is to stimulate the myosin ATPase activity. Myosin-S1 of skeletal or cardiac muscle represents the globular N-terminal domain of myosin that contains both the actin binding and the separate ATPase site. Our data show that every c-α-actin isoform was able to stimulate the myosin-S1 ATPase in a concentration dependent manner (see Fig. S3). Decoration with cTm/cTn led to an increase of the myosin-S1 ATPase stimulatory activity of wt, p.A295S and p.E361G c-α-actin probably due to stabilisation of the filament structure as indicated by EM, except for the p.R312H mutant (see Fig. S3) that also after cTm/cTn decoration retained a wavy structure and whose myosin-S1 stimulatory activity did not increase after cTm/Tn decoration (Fig. 4). Previously, a similar behaviour of the p.R312H mutant has been reported that was releated to a reduced stability [41,67]. These effects are reflected by the kinetic parameters (see Table S1), which in particular indicate a higher myosin-S1 ATPase stimulatory capacity ($V_{max}$) of p.A295S after decoration with cTm/cTn than wt and the DCM c-α-actin variants (Table S1).

Decoration of all c-α-actin variants with cTm/cTn conferred $Ca^{2+}$-sensitivity of their myosin-S1 ATPase stimulatory activity underlining their full functionality. Slight differences in the $pCa_{50}$ were observed. The p.A295S HCM mutant showed an at least equal or slightly higher $Ca^{2+}$-sensitivity than wt c-α-actin, which was clearly higher than that of the two DCM variants (see Tables 3 and 4). The data are in line with the assumption that HCM is correlated with a high and DCM with decreased $Ca^{2+}$-sensitivity leading to a higher myosin-ATPase activity already at low $Ca^{2+}$-concentration [62].

The $pCa_{50}$ differences between the c-α-actins were principally maintained when determining the fluorescence increase of pyrene-cTm presumably paralleling the cTm movement from the C- to M-state though it occurred at lower $Ca^{2+}$-ion concentrations (Fig. 6 and Table 4). The reasons for this difference are presently not clear. It is possible that an internal conformational change of pyrene-cTm leads to an earlier response of the fluorescent eximer [25]. Using this procedure the p.A295S mutant showed the highest $Ca^{2+}$-sensitivity in the presence of only myosin-S1 (Fig. 6E), whereas that of the p.R312H and p.E361G mutants was lower than of recombinant wt c-α-actin (Fig. 6E and Table 4). Thus these data are in agreement with the notion that HCM or DCM are correlated with and increased or decreased myosin activity, respectively [56, ].

In these measurements we also included the N-terminal fragment C0C2 of cMyBP-C. MyBP-C was first discovered in skeletal muscle bound to the thick filaments, where it is restricted to the overlap region of thick and thin filaments [43]. MyBP-C is able to attach also to actin and titin thereby connecting thin and thick filaments. Meanwhile three isoforms of MyBP-C were identified: skeletal, smooth and cardiac muscle specific isoforms [51,57]. Cardiac MyBP-C is composed of eight immunoglobin-like and three fibronectin-like domains, which are numbered from C0 (N-terminus) to C10 [51]. C0 and C1 are linked by a flexible proline-alanine rich linker and between C1 and C2 is placed the M-domain, which is phosphorylated by a number of signalling protein kinases [51,57]. In our experiments we used the N-terminal and actin-binding fragment C0-C2 of cardiac MyBP-C, which has been shown to broaden the $Ca^{2+}$-response (decrease of the Hill coefficient) and thereby to increase the $Ca^{2+}$-sensitivity of native thin filaments at low $Ca^{2+}$-concentrations [51]. Due to its recombinant expression the C0C2-fragment was non-phosphorylated and probably unable to bind myosin-S1.

Our data show N-cMyBP-C was able to increase the $Ca^{2+}$-sensitivity of bovine and wt c-α-actin both in the absence and presence of myosin-S1, whereas its effect on the mutant c-α-actins varied from none to a slight increase in $Ca^{2+}$-sensitivity of p.R312H and p.E361G in the absence of myosin-S1 (Table 4). These different responses might be due to alterations of the interaction of N-cMyBP-C with the mutated actins. Indeed, previous data have shown that the affinity of the C0C2 fragment is reduced to mutated c-actins especially to the p.E361G mutant [9], because this mutation in subdomain 1 might be located close to the presumed binding region of N-cMyBP-C [51]. Nevertheless, it appeared that in the presence of myosin-S1 N-cMyBP-C shifted the $Ca^{2+}$-sensitivity of p.A295S below that of wt (compare Fig. 6E with 6F) suggesting that it might reduce deleterious effects of c-actin mutants.

Finally, we tested the behaviour of the cardiac actins when transfected into established cell lines or rat neonatal cardiomyocytes. The transfection of non-muscle cell lines indicated incorporation of all c-α-actins into the cellular cytoskeleton though we noted a preference of wt and p.A295S c-α-actins for the microfilament system, whereas the p.R312H and E361G mutants incorporated into the submembranous cortical F-actin network, a behaviour more typical of cytoplasmic actins. This might appear surprising, since the six mammalian actins contain identical residues at positions 295, 312, and 361 (A, R and E, respectively). Therefore the mutations at the positions 312 and 361 might have reduced the strength of

their interactions with filament forming actin binding proteins, especially of the p.E361G mutant, whose rate of polymerization was not stimulated by mDia3-FH2 (Fig. 3).

In contrast, after transduction of neonatal rat cardiomyocytes (NRCs) the c-α-actin variants were found to form or incorporate into sarcomeric structures (Fig. 7,8). A clear separation, however, of the intracellular localisation of exogenous and endogenous c-actins was found in one to two days old NRCs. These cells showed a more central localisation of the exogenous actins, irrespective of the variant, in sarcomeric and microfilamentous organisations, and a peripheral of the endogenous c-α-actin in sarcomeric form (Fig. 7A). Sarcomerogenesis has been shown to start at the cell periphery at sites of attachment to the extracellular matrix and to subsequently extend centripetally [8]. These sites (also termed proto-costameres) might have been initiated and developed before translation of the adenovirally introduced exogenous c-α-actin variants. It is also possible that the mRNA of endogenous c-α-actin contained additional localisation signals that directed its translation to the cell periphery and therefore attracted preferentially newly formed endogenous c-α-actins [31]. Such signals were absent in the adenoviral constructs.

Finally, we determined the site of incorporation of the exogenous c-α-actins into the sarcomeric thin filaments by co-staining with anti-α-actinin and -myomesin, markers of the Z- and M-line, respectively. All c-α-actins appeared to incorporate at the Z-line, i.e. the thin filament plus end, except the p.E361G mutant, which preferentially incorporated in the region of the M-line. The p.E361G residue is localised in subdomain 1 of actin and has been implicated in binding to α-actinin [65]. This mutation has been shown to reduce its affinity α-actinin [65] and thereby impairs filament plus end incorporation. However, the immunostaining showed a weak HA-p.E361G immunostaining between the myomesin bands indicating albeit reduced plus-end incorporation.

# Conclusions

In summary, our data show that recombinant wt c-α-actin behaved very similar to conventionally purified bovine c-α-actin. This concordance strengthens the assumption that the isolated mutant c-α-actins were also in native state and exhibited their intrinsic functionality. Our results describe a number of differences of the c-actin mutants in their biochemical and cell biological behaviour. It can be stated that each variant showed individual differences:

**The HCM p.A295S mutant** showed an EM appearance and polymerizability similar to wt c-actin, but was less efficiently stimulated by Arp2/3 complex but stronger by mDia3-FH2 than wt c-actin, a behaviour that might lead to its preferable incorporation into stress fibre systems. In agreement with previous reports we also observed that p.A295S possessed a slightly higher $Ca^{2+}$-sensitivity and stimulatory activity of the myosin-S1 ATPase than the other c-actins [64]. It has been proposed that its higher $Ca^{2+}$-sensitivity was due to a charge disturbance of the A-triad, since residue 295 is located on a helix opposite the A-triad containing loop [27,32,36]. The A-triad is a sequence of positvely charged residues (K326, K328, and R147) that is implicated in stabilising tropomysin binding in the closed-blocked (C,B) position. Since

residue A295 is in close vincinity to the A-triad, the alanine to serine mutation may distort the positive charge patch of the A-triad and lead to the observed higher $Ca^{2+}$-sensitivity of cTm movement in the presence of myosin-S1. This behaviour agrees with the current hypothesis that HCM is caused by a hypercontractility. Our data however show that in the absence of myosin-S1 or the presence of N-cMyBP-C this effect is less pronounced suggesting that this effect might be restricted to the MyBP-C free overlap region, i.e. to both sides of the Z-line, the region of p.A295S incorporation.

One pecularity of the DCM **p.R312H mutant** was its steep increase in the $Ca^{2+}$-sensitivity and Hill coefficient (of 3.9), that was however considerably reduced by myosin-S1 and not observed in the ATPase measurements (Fig. 5). The p.R312H residue is located in subdomain 3 of actin (Fig. 1) and close to the A-triad that is involved in electrostatic binding of tropomyosin [13,36]. Furthermore, the neighbouring residue D311 forms the strongest electrostatic contact to Tm [13]. Therefore a mutation leading to a reduction of positive charges of this region might lead to reduced affinity of the p.R312H mutant to cTm and be the reason for the high Hill coefficient (of 3.9) observed in the pyrene-cTm measurement indicative for a low energy barrier of the transition from B- to M-state (Table 4) [11]. In agreement with previous reports [36,64] the DCM p.R312H mutant showed a reduced polymerizability (Fig. 3C), though positively affected by the nucleators. Interestingly another recently detected amino acid exchange at this position, the p.R312K variant, did not affect actin polymerization, but was not influenced by the two nucleators (see Supplementary Information). EM indicated that p.R312H-actin filaments were wavy and showed strand breaks that were still observed after decoration with cTm/Tn. Both results suggested reduced stability of p.R312H filaments, which might explain the observation that decoration with cTm/Tn did not further increase its myosin-S1 ATPase stimulatory capacity. In the presence of both myosin-S1 and N-cMyBP-C the $Ca^{2+}$-sensitivity decreased slightly most probably due to their simultaneous binding to cTm and c-actin (Table 4). It appears however probable that the reduced filamentous stability of p.R312H c-actin leading to reduced myosin-S1 ATPase activation might be causative for DCM development.

The **DCM p.E361G mutation** is located in subdomain 1 the binding region of myosin heads and α-actinin [5,67]. The p.E361G mutation is reported to cause a three fold lower affinity to α-actinin [67] that might be responsible for its preferred incorporation into into cytoskeletal F-actin networks of culture cells and the thin filament minus-ends, although a small fraction was observed to also incorporate into the plus-ends (Fig. 8M). This might lead to a reduction of the stability of the attachment of thin filaments to the Z-lines. Indeed, it was observed that the hearts of transgenic mice expressing the E361G mutant developed contractile dysfunction under stress and signs of DCM [55], although this mutant showed a high rate of polymerization that was not further stimulated by Arp2/3 complex and mDia3-FH2.

Furthermore, previous investigations have shown that the p.E361G mutation abolishes the $Ca^{2+}$-ion regulatory effect of cTnI phosphorylation [55]. Phosphorylation of two N-terminal serines of cTnI by protein kinase A (PKA) after ß1-adrenergic stimulation increases the $Ca^{2+}$-sensitivity and by interaction with TnC the rate $Ca^{2+}$-dissociation and subsequently the heart rate [55,66]. The p.E361G mutant was shown to blunt the increase in $Ca^{2+}$-sensitivity affected cTnI phosphorylation, thereby the adrenergic

responsiveness of cardiac muscle is lost leading to a decrease of its $Ca^{2+}$-sensitivity further supporting the development of DCM [55].

In summary, our data indicate that each c-actin mutation possesses its own specific alterations in the mode of interactions with particular sarcomeric proteins. Apart from the general accepted notion that alterations in the $Ca^{2+}$-sensitivity affecting the contractlity can lead to either HCM or DCM, our data demonstrate that modifies interactions of mutant c-actins with other sarcomeric proteins during development and in adult cardiac muscle may also play an essential role for CM establishment.

## Declarations

# Acknowledgement:

The financial support by the Deutsche Forschungsgemeinschaft (DFG: Ma807/19-1), and the German Academic Exchange Service (DAAD), Bad-Godesberg, Germany, for RH are gratefully acknowledged.

# Conflicts of interest/Competing interests:

The authors declair no conflicts of interests.

# Availability of data and material

# Code availability

(software application or custom code)

# Authors' contributions:

All authors contributed to the study conception and design. Material preparation, data collection and analysis were performed by C. Erdmann, R. Hassoun, S. Schmitt, S. Fujita-Becker, A.J. Mazur, and H.G. Mannherz. The first draft of the manuscript was written by H.G. Mannherz and all authors commented on previous versions of the manuscript. All authors read and approved the final manuscript.

## References

1. Babu A, Scordilis SP, Sonnenblick EH & Gulati J (1987) The control of myocardial contraction with skeletal fast muscle troponin. J Biol Chem 262: 5815–5822.
2. Bai F, Caster HM, Rubenstein PA, Dawson JF, and Kawai M (2014) Using baculovirus/insect cell expressed recombinant actin to study the molecular pathogenesis of HCM caused by actin mutation

A331P. J Mol Cell Cardiol 74: 64-75.

3. Barry SP, Davidson SM, Townsend PA (2008) Molecular regulation of cardiac hypertrophy. The International J Biochem Cell Biol 40: 2023–2039.
4. Bailey K (1948) Tropomyosin: a new asymmetric protein component of the muscle fibril. Biochemical Journal 43(2): 271-279
5. Behrmann E, Müller M, Penczek PA, Mannherz H G, Manstein DJ, Raunser S (2012) Structure of the rigor actin-tropomyosin-myosin complex. Cell 150: 327–338.
6. Bookwater CS, Trybus KM (2006) Functional consequences of a mutation in an expressed human alpha-cardiac actin at a site implicated in familial hypertrophic cardiomyopathy. J Biol Chem 28: 16777-84.
7. Bradford MM (1976) A rapid and sensitive method for the quantitation of microgram quantities of protein utilizing the principle of protein-dye binding. Anal Biochem 72: 248–254.
8. Chobra A, Kutys ML, Zhang K, Polacheck WJ, Sheng CC, Luu RJ, Eyckmans J, Hinson JT, Seidman JG, Seidman CE, Chen CS (2018) Force generation via β-cardiac myosin, titin, and α-actinin drives cardiac sarcomere assembly from cell-matrix adhesions. Dev Cell 44: 87-96.
9. Chow ML, Shaffer JF, Harris SP, Dawson JF (2014) Altered interactions between cardiac myosin binding protein-C and α-cardiac actin variants associated with cardiomyopathies. Arch Biochem Biophys 15: 28-32.
10. Cimiotti D, Fujita-Becker S, Möhner D, Smolina N, Budde H, Wies A, Morgenstern L, Gudkova A, Sejersen T, Sjöberg G, Mügge A, Nowaczyk MM, Reusch P, Pfitzer G, Stehle R, Schröder RR, Mannherz HG, Kostareva A, Jaquet K (2020) Infantile restrictive cardiomyopathy: CtnI-R170G/W impair the interplay of sarcomeric proteins and the integrity of thin filaments. PLoS One. 15(3): e0229227, doi: 10.1371/journal.pone.0229227.
11. Debold EP, Saber W, Cheema Y, Bookwalter CS, Trybus KM, Warshaw DM, Vanburen P (2010) Human actin mutations associated with hypertrophic and dilated cardiomyopathies demonstrate distinct thin filament regulatory properties in vitro. J Mol Cell Cardiology 48: 286–292.
12. Deng Y, Schmidtmann A, Redlich A, Westerdorf B, Jaquet K, Thieleczek R (2001) Effects of Phosphorylation and Mutation R145G on Human Cardiac Troponin I Function. Biochemistry 40: 14593-14602.
13. Ebashi S, Endo M, Otsuki I (1969) Control of muscle contraction. Rev Biophys 2:351–384.
14. Ehler E, Moore-Morris T, Lange S (2013) Isolation and culture of neonatal mouse cardiomyocytes. J Vis Exp 50154.
15. Ehler E (2018) Actin-associated proteins and cardiomyopathy-the ‘unknown’ beyond troponin and tropomyosin. Biophys Rev 10(4): 1121–1128.
16. Erdmann C (2017) Charakterisierung von HCM und DCM auslösenden Mutationen in humanem kardialem α-Aktin. PhD-thesis, Ruhr-University Bochum.

17. Fananapazir L (2000) Inherited and de novo mutations in the cardiac actin gene cause hypertrophic cardiomyopathy. J Mol Cell Cardiology 32: 1687–1694.
18. Feng JJ, Marston S (2009) Genotype–phenotype correlations in ACTA1 mutations that cause congenital myopathies. Neuromus Disorders 19: 6–16.
19. Geeves MA, Lehrer SS (1984) Dynamics of the muscle thin filament regulatory switch: the size of the cooperative unit. Biophys J 67(1): 273–282.
20. Geeves MA, Lehrer SS, Lehman W (2019) The mechanism of thin filament regulation: Models in conflict. J Gen Physiol 151: 1265- 1271.
21. Graceffa P, Lehrer SS (1980) The eximer fluorescence of pyrene-labeled tropomyosin: A probe for conformational dynamics. J Biol Chem 255: 11296-11300.
22. He T-C, Zhou S, da Costa LT, Yu J, Kinzler KW, Vogelstein B (1998) A simplified system for generating recombinant adenoviruses. Proc Natl Acad USA 95(5): 2509–2514.
23. Herman DS, Lam L, Taylor MRG, Wang L, Teekakirikul P, Christodoulou Conner DL, Steven R. McDonough DB, Sparks E, et al (2012) Truncations of Titin causing Dilated Cardiomyopathy. New Engl J Medicine 366: 619-628.
24. Hesterkamp T, Weeds AG, Mannherz HG (1993) The two actins of the gelsolin:2 actin complex are in antiparallel orientation. Eur J Biochem 318: 507-513.
25. Ishii Y, Lehrer SS (1990) Excimer fluorescence of pyrenyliodoacetamide- labeled tropomyosin. Biochemistry 29: 1160-1166.
26. Jahn W (1995) Easily prepared holey films for use in cryo-electron microscopy. J Microscopy 179: 333–334.
27. Kabsch W, Mannherz HG, Pai E, Suck D, Holmes KC (1990) The atomic structure of actin:DNase I complex. Nature 347: 37-44.
28. Kouyama T, Mihashi K (1981) Fluorimetry study of N-(1-pyrenyl) Iodoacetamide-labelled F-actin. Local structural change of actin protomer both on polymerization and on binding of heavy meromyosin. Eur J Biochem 114: 33–38.
29. Kühn S, Geyer M (2014) Formins as effector proteins of Rho GTPases. Small GTPases 5: e29513.
30. Laemmli UK (1970) Cleavage of structural proteins during the assembly of the head of bacteriophage T4. Nature 227: 680-685.
31. Lawrence JB, Singer RH (1986) Intracellular localization of messenger RNAs for cytoskeletal proteins. Cell 45:407–415.
32. Lehman W, Rynkiewicz MJ, Moore JR (2020) A new twist on tropomyosin binding to actin filaments: perspectives on thin filament function, assembly and biomechanics J Muscle Res Cell Motility 41: 23-38
33. Lynn ML, Lehman SJ, Tadiff JC (2018) Biophysical Derangements in Genetic Cardiomyopathies. Heart Failure Clin. 14: 147-159.

34. Mannherz HG, Brehme H, Lamp U (1975) Depolymerization of F-actin and its repolymerization in the presence of analogs of adenosine triphosphate. Eur J Biochem 60: 109-116.
35. Mannherz HG, Goody, R.S., Konrad, M., and Nowak, E. (1980) The interaction of pancreatic deoxyribonuclease I and skeletal muscle actin. Eur J Biochem 104: 367-379.
36. Marston SB (2011) How do mutations in contractile proteins cause the primary familial cardiomyopathies? J Cardiovascular Translational Res 4: 245–255.
37. Mazur AJ (2008) Expression of constructs of WT-alpha-cardiac actin and its mutants in different cell lines and primary rat cardiac myocytes. PhD-thesis, Ruhr-University Bochum.
38. Moreno Gonzales A, Drapala P, Kruetziger K, Regnier M (2003) Decreased Ca2+ binding by troponin C isoforms enhances crossbridge contribution to thin filament activation. Biophys J 84: 449a.
39. Müller M, Mazur JA, Behrmann E, Diensthuber RP, Radke MP, Qu Z, Littwitz C, Raunser S, Schoenenberger C-A, Manstein DJ, Mannherz HG (2012) Functional characterization of the human α-cardiac actin mutations Y166C and M305L involved in hypertrophic cardiomyopathy. Cellul Molec Life Sci 69; 3457-3479.
40. Mogensen J, Perrot A, Andersen PS, Havndrup O, Klausen IC, Christiansen M, Bross P, Egeblad H, Bundgaard H, Osterziel KJ, Haltern G, Lapp H, Reineke P, Gregersen N, Borglum AD (2004) Clinical and genetic characteristics of alpha cardiac actin gene mutations in hypertrophic cardiomyopathy. J Med Genet 41: e10, doi 10.1136/jmg 2003.010447.
41. Mundia MM, Demers RW, Chow ML, Perieteanu AA, Dawson JF (2012) Subdomain location of mutations in cardiac actin correlate with type of functional change. Plos ONE 7: e3621.
42. Ohki T, Ohno C, Oyama K, Mikhailenko SV, Ishiwata S (2009) Purification of cytoplasmic actin by affinity chromatography using the C-terminal half of gelsolin. Biochem Biophys Res Commun 383: 146–150.
43. Offer G (2015) Myosin-binding protein-C: bridging the gap. J Mol Biol 427: 231- 235.
44. Olson TM, Michels VV, Thibodeau SN, Tai Y-S, Keating MT (1998) Actin mutations in Dilated Cardiomyopathy, a heritable Form of Heart failure. Science 280: 750-752.
45. Olson TM, Doan TP, Kishimoto NY, Whitby FG, Ackerman MJ, Fananapazir L (2000) Inherited and de novo Mutations in the cardiac actin gene cause hypertrophic cardiomyopathy. J Mol Cell Cardiol 32: 1687- 1694.
46. Parker F, Baboolal TG, Peckham M (2020) Actin mutations and their role in disease. Int. J Sciences 21: 3371-3387.
47. Qu Z, Silvan U, Jockusch BM, Aebi U, Schoenenberger CA, Mannherz HG (2015) Distinct oligomers modulate differently the activity of actin nucleators. FEBS J 282(19): 3824-3840.
48. Qu Z, Fujita-Becker S, Ballweber E, Ince S, Herrmann C, Schröder RR, Mannherz HG (2018) Interaction of isolated cross-linked short actin oligomers with the skeletal muscle myosin motor domain. FEBS J 285(9):1715-1729. doi: 10.1111/febs.14442.

49. Reiffert S, et al., Characterization of the cardiac holotroponin complex reconstituted from native cardiac troponin T and recombinant I and C. The FEBS Journal, 1999. 261(1): p. 40-47
50. Reinecke P, Gregersen N, Børglum AD (2004) Clinical and genetic characteristics of alpha cardiac actin gene mutations in hypertrophic cardiomyopathy. J Medical Genetics 41: e10.
51. Risi C, Belknap B, Forgacs-Lonart E, Harris SP, Schröder GF, White HD, Galkin VE (2018) N-terminal domains of cardiac myosin binding protein C cooperatively activate the thin filament. Structure 26: 1-8.
52. Rosado M, Barber CF, Berciu C, Feldman S, Birren SJ, Nicastro D, Good BL (2014) Critical roles for multiple formins during cardiac myofibril development and repair. Mol Biol Cell 25(6): 811–827.
53. Sabater-Molina M, Pérez-Sánchez I, Hernández Del Rincón JP, Gimeno JR (2017) Genetics of hypertrophic cardiomyopathy: a review of current state. Clinical Genetics 93: 3-14.
54. Seidman JG, Seidman C (2001) The genetic basis for cardiomyopathy: from mutation identification to mechanistic paradigms. Cell 104: 557–567.
55. Song W, Dyer E, Stuckey D, Leung M-C, Memo M, Mansfeld C, Ferenci M, Liu K, Redwood C, Nowak K, Harding S, Clarke K, Wells D, Marston S (2010) Investigation of a transgenic mouse model of familial dilated cardiomyopathy. J Mol Cell Cardiol 49: 380-389.
56. Spudich JA (2015) The myosin mesa and a possible unifying hypothesis fort he molecular basis of human hypertrophic cardiomyopathy. Biochem Soc Trans 43: 64-72.
57. Starr R, Offer G (1978) The interaction of C-protein with heavy meromyosin and subfragment 2. Biochem J 171: 813-816.
58. Tanaka H, Sekine T, Kawanishi T, Nakamura R, Shigenobu K (1998) Intrasarcomere [$Ca^{2+}$] gradients and their spatio-temporal relation to $Ca^{2+}$ sparks in rat cardiomyocytes. J Physiol 508: 145-152.
59. Tayler RS, Weeds AG (1976) The magnesium-ion-dependent adenosine triphosphatase of bovine cardiac Myosin and its subfragment-1. Biochem J 159: 301-315.
60. Towbin H, Staehelin T, Gordon J (1979) Electrophoretic transfer of proteins from polyacrylamide gels to nitrocellulose sheets: procedure and some applications. Proc Nat Acad Sci USA 76: 4350–4354.
61. Trentham DR, Bardsley RG, Eccleston JF, Weeds AG (1972) Elementary processes of the magnesium ion-dependent adenosine triphosphatase activity of heavy meromyosin. A transient kinetic approach to the study of kinases and adenosine triphosphatases and a colorimetric inorganic phosphate assay in situ. The Biochem J 126: 635–644.
62. Trivedi DV, Adhikari AS, Sarkar SS, Ruppel KM, Spudich JA (2018) Hypertrophic cardiomyopathy and the myosin mesa: viewing an old disease in a new light. Biophys Rev 10: 27–48.
63. von der Ecken J, Müller M, Lehman W, Manstein DJ, Penczek PA, Raunser S (2015) Structure of the F-actin-tropomyosin complex. Nature 519: 114–117.
64. Viswanathan MC, Schmidt W, Rynkiewivz MJ, Agarwal K, Gao J, Katz J, Lehman W, Cammarato A (2017) Distortion of the actin A-triad results in contractile disinhibition and cardiomyopathy. Cell Reports 20: 2612-2625.

65. Vikhorev PG, Song W, Wilkinson R, Copeland O, Messer AE, Ferenczi MA, and Marston SB (2014) The Dilated Cardiomyopathy-Causing Mutation ACTC E361G in Cardiac Muscle Myofibrils Specifically Abolishes Modulation of $Ca^{2+}$ Regulation by Troponin I. Biophys J 107: 2369–2380.
66. Weintraub RG, Semsarian C, Macdonald P (2017) Dilated cardiomyopathy. Lancet (London, England) 390: 400-414.
67. Wong WW, Doyle TC, Cheung P, Olson TM, Reisler E (2001) Functional studies of yeast actin mutants corresponding to human cardiomyopathy mutations. J Muscle Res Cell Motil 22: 665-674.

# Figures

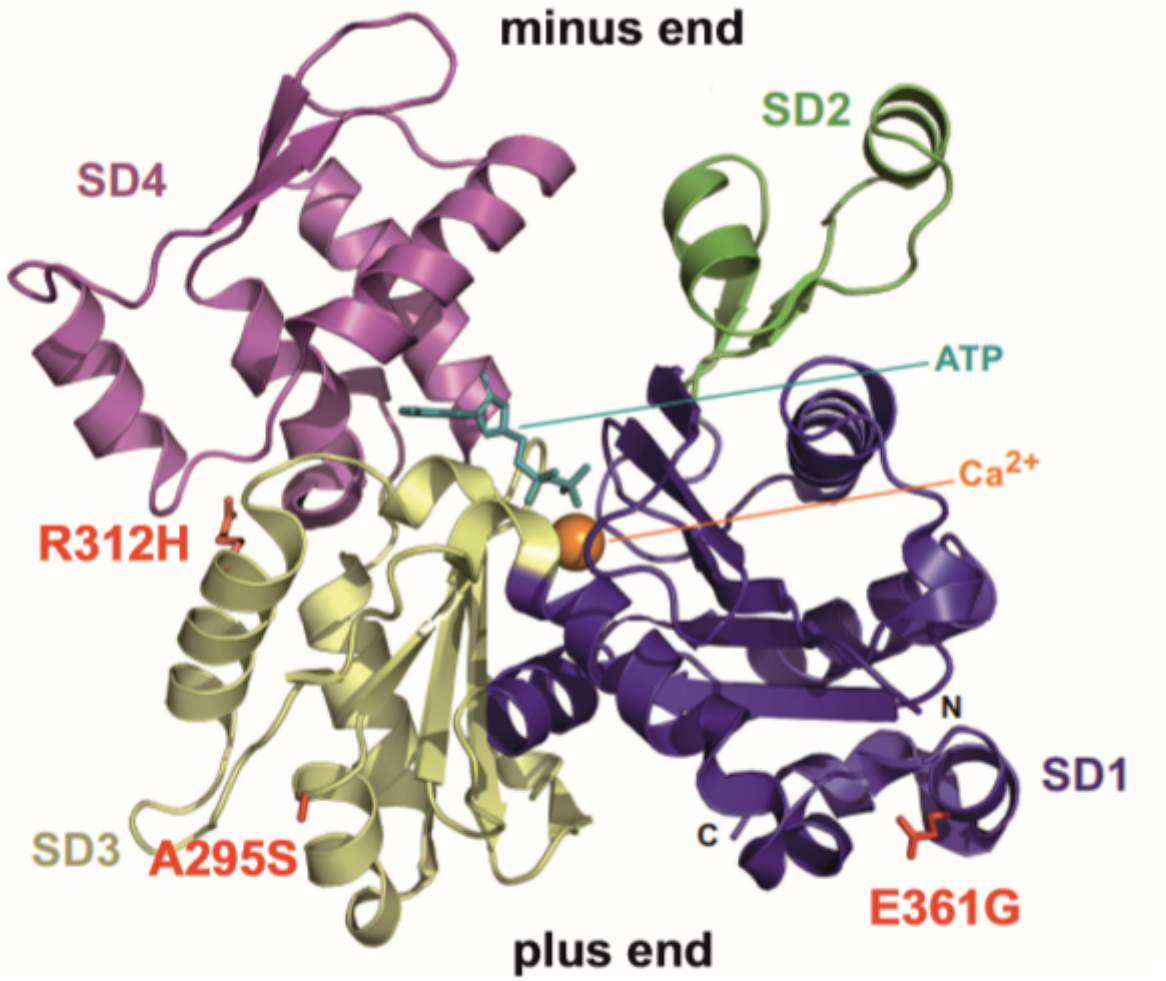


**Figure 1**

3D structural model of G-actin derived from the skeletal muscle actin:DNase I complex [27] indicating the positions of the mutated residues of the c-actin mutants investigated. In addition subdomains (SD) as well as the position of ATP and Ca2+ are indicated.

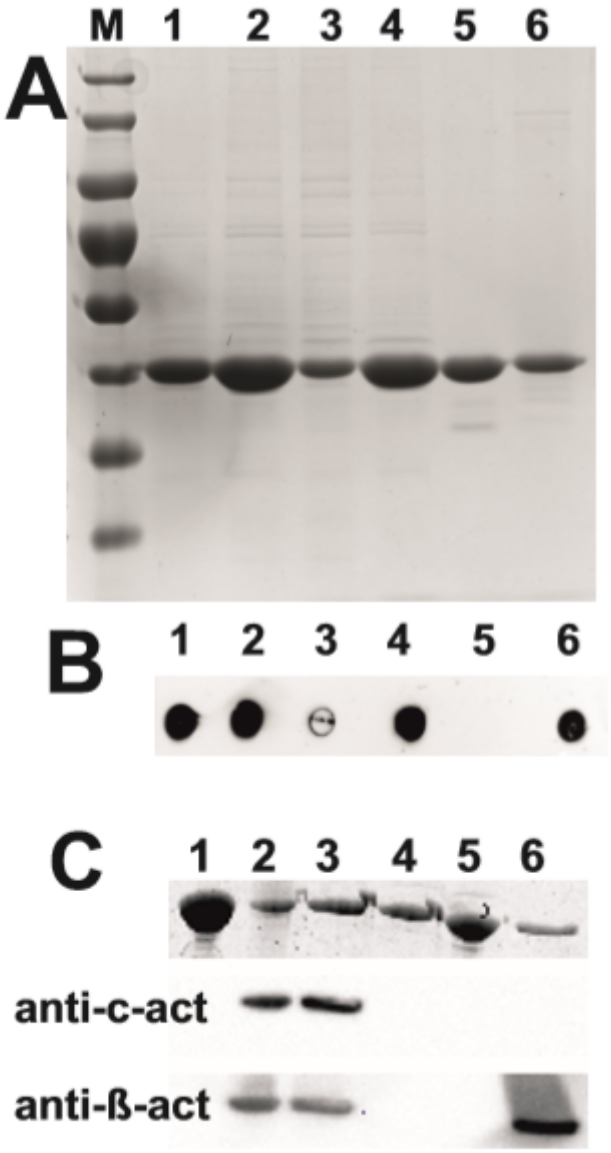


## Figure 2

Purification of cardiac actins after expression by the baculovirus/Sf21 system. (A) SDS-Page of the purified cardiac actin variants used in this study. Lanes: (1) wt; (2) p.A295S; (3) p.R312K; (4) p.E361G; (5) skeletal muscle actin; and (6) bovine cardiac actin. Actins shown in lanes (5) and (6) were conventionally prepared from acetone powders. (B) Dot immunoblots of the actins shown in (A) using the anti-cardiac actin monoclonal antibody. Note that the p.R312K mutant is only weakly and skeletal muscle actin is not stained by anti-c-actin maB. (C) Upper row: SDS-Page of the following actins: Lanes: (1) skeletal muscle actin (2) wt cardiac actin (recombinant); (3) bovine cardiac actin; (4) cytoplasmic γ-actin; (5) actin purified from Acanthameba castellani; and (6) cytoplasmic β-actin. Middle row: Western blot of the SDS-Page immunostained with anti-cardiac actin mAB; and (lower row) with anti-β-actin mAB. Note that only the cardiac actins (recombinantly expressed wt and the conventionally prepared bovine c-actin) are immunostained by anti-c-actin maB and additionally exhibit β-actin immunoreactivity.

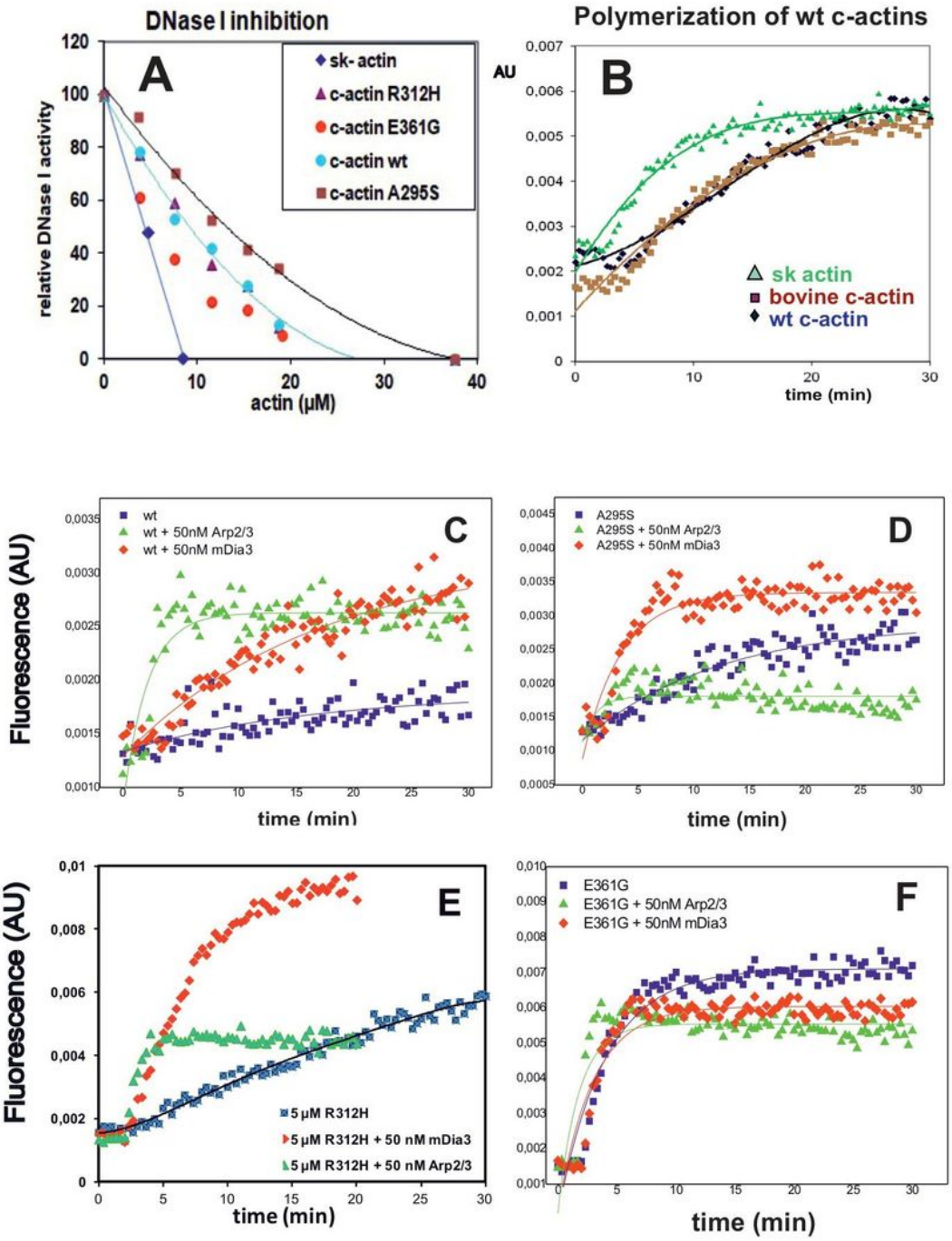


## Figure 3

Properties of the purified c-actins indicating native state (A) Inhibition of DNase I activity as measured by the hyperchromicity assay. Human DNase I (0.1 µg/µl = 3.12 µM) was mixed with the amounts of c-actins indicated in the abscissa. DNase activity was determined as detailed [35]. Ordinate gives the relative remaining activity calculated. (B to F) Actin polymerization after addition of 2 mM MgCl2 at t = 2 min as determined by the pyrene-assay using 0.5 µM pyrene-labelled skeletal muscle actin (see Materials and

methods). (B) Comparison of purified sk-actin and bovine c-actin purified from acetone powders with recombinant wt c-actin, each at 5 μM Note the faster polymerization rate of sk-actin and the equal rates of c-actins. (C to F) Influence of nucleators on the rates of polymerization of c-actins. (C) Recombinant wt-c-actin, (D) p.A295S, (E) p.R312H, and (F) p.E361G. All c-actins at 5 μM and in the absence of presence of either 50 nM Arp2/3 complex or 50 nM mDia3-FH2 (for details see text).

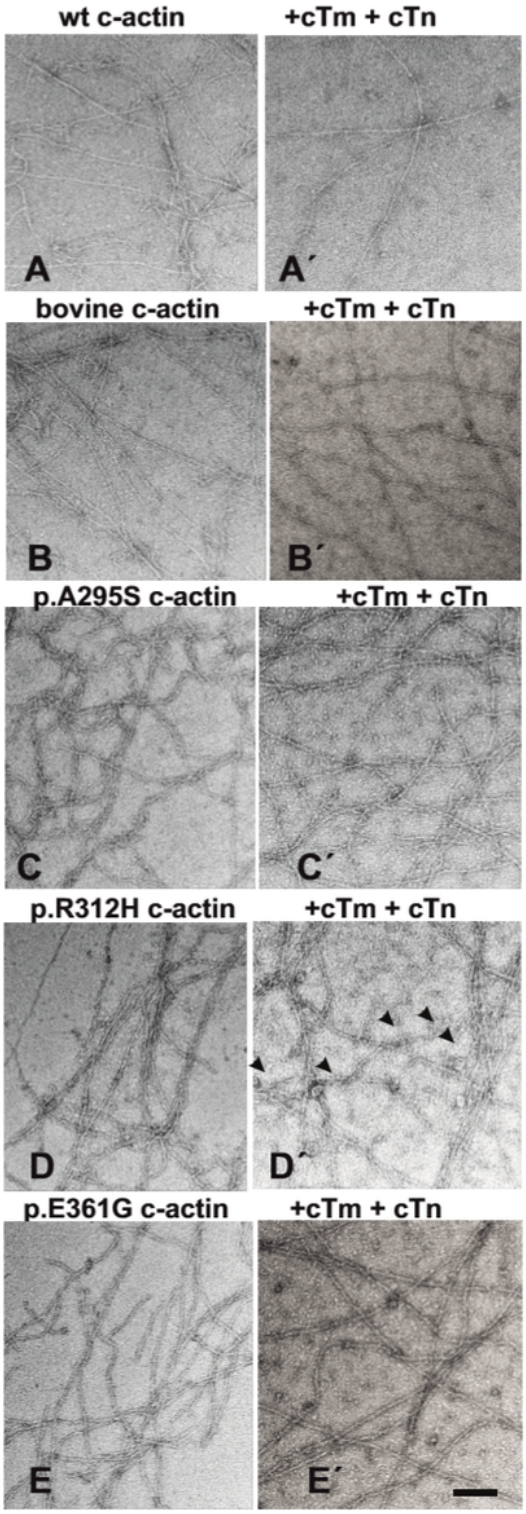


## Figure 4

EM analysis after negative staining of the polymerized c-actins before and after decoration with cTm and cTn at a 7:1:1 molar ratio. (A,A´) Wt recombinant c-actin, (B,B´) bovine c-actin, (C,C´) p.A295S, (D,D´) p.R312H (arrow heads point to strand breaks and wavy filaments), and (E,E´) p.E361G. Scale bar in (E´) = 100 nm (applicable to all images).

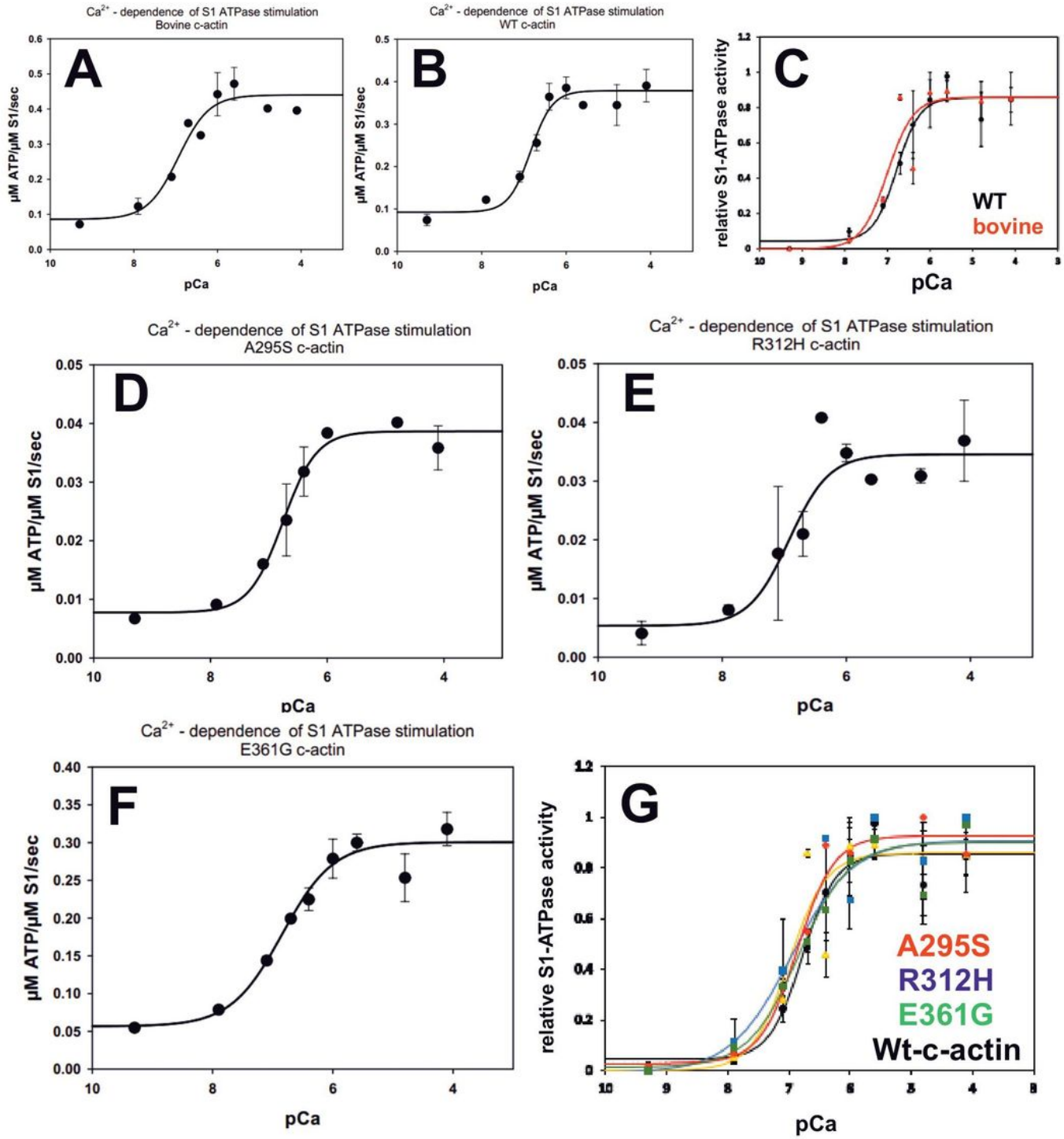


Figure 5

Ca2+-concentration dependence of the stimulation of the myosin-S1 ATPase by c-actins decorated with cTm and cTn at 6:1:1 molar ratio. Skeletal muscle myosin-S1 ATPase activity was determined by the enzyme-linked assay. ATPase stimulation by (A) recombinant wt c-actin, (B) bovine c-actin, and (C) comparison of (A) and (B). ATPase stimulation by (D) p.A295S, (E) p.R312H, and (F) p.E361G. (G) Comparison of the mutant forms of c-actin. Final F-c-actin concentrations in assay were 1.5 μM and of rabbit skeletal muscle myosin-S1 0.5 μM. ATPase activity (ordinate) is given as μM ATP hydrolysed/sec/μM myosin-S1 in (A;B;D-F) and normalized in (C and G) setting the minimal ATPase activity (generally at pCa 9.3) as zero and the maximal at 1 (generally at pCa 4.8). Abscissa gives pCa-values (-log molar Ca2+-concentration). All measurements were performed in triplicate.

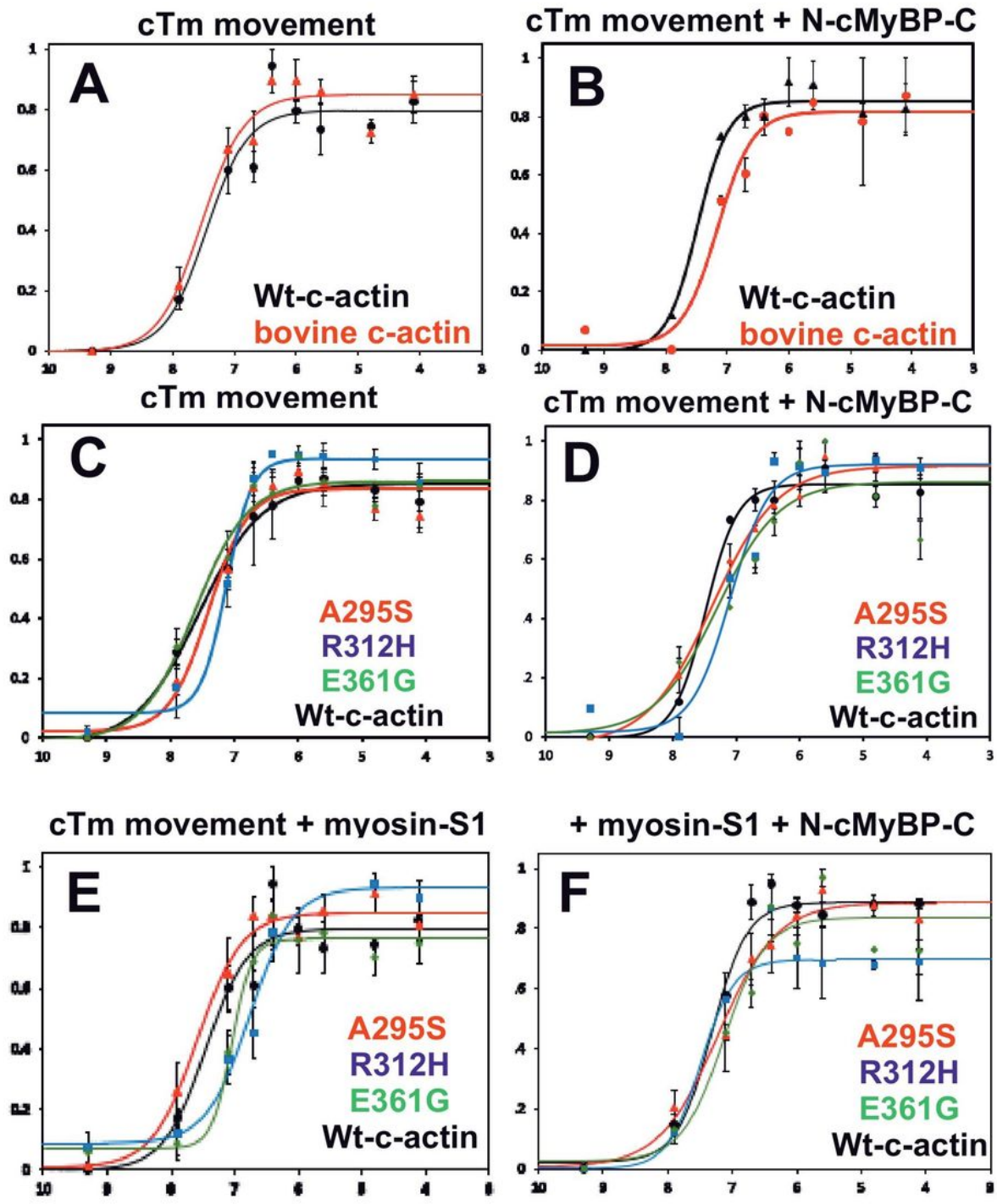


## Figure 6

Comparison of the Ca2+-concentration dependence of the fluorescence increase (movement) of pyrene-labelled cTm on bovine and recombinant c-actin variants. Pyrene-labelled cTm was used to determine its movement along filamentous bovine and recombinant wt c-actin (for details see text). The c-actins (final concentration in microtiter plate 0.4 µM) were decorated with pyrene-labelled cTm and cTn at a molar ratio of 6:1:1 (see Materials and methods) and the Ca2+-dependence of the fluorescence increase of the

pyrene-labelled cTm corresponding to Tm-movement was determined using a Tecan Elisa-reader as detailed in Materials and methods [10]. (A) Comparison of bovine c-actin and recombinant wt c-actin decorated with pyrene-cTm and cTn in the absence and (B) the presence of N-cMyBP-C. (C,D) Identical experiment to (A) and (B) using the recombinant c-actins. (E,F) Identical experiment to (C) and (D) using the recombinant c-actins in the additional presence of myosin-S1. The ordinates give the fluorescence intensities (F) normalized to Fmax = 1, Fmin = 0. and abscissa the pCa (for compilation of data see also Table 4). The colour coding for the c-actins is given in the Figure.

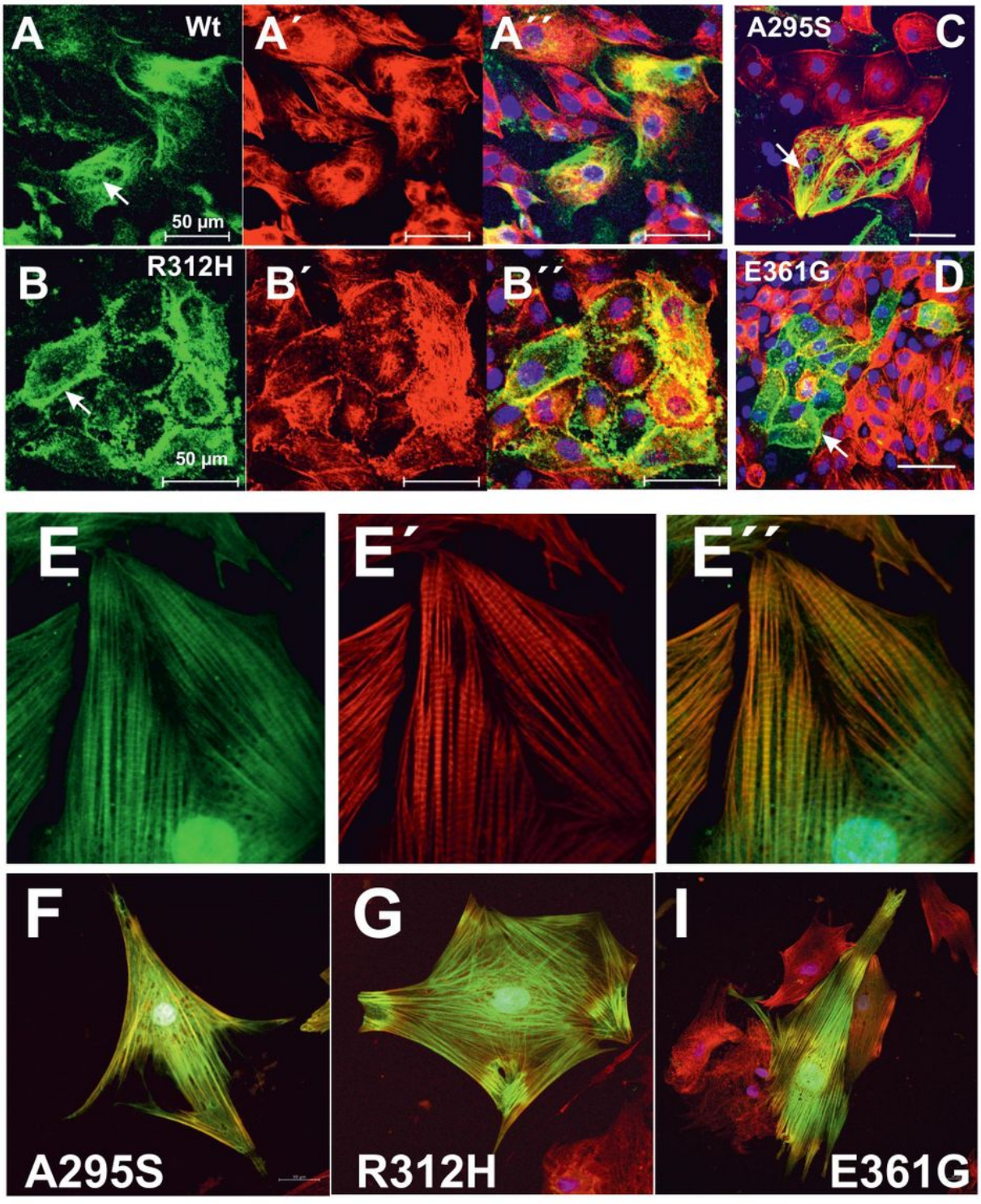

## Figure 7

Transfection of MDCK cells with HA-tagged c-actin variants. The MDCK cells were transfected with vectors containing HA-tagged c-actin variants (for details see Materials and Methods). Subsequently the cells were immunostained with anti-HA and counterstained with TRITC-phalloidin. (A) wt c-actin stained with anti-HA (green); (A´) TRITC-phalloidin staining; (A´´) merge. (B-B´´) Identical staining for the p.R312H mutant. (C) Merged image of identical staining of p.A295S and (D) of the p.E361G mutant. Note for wt and the p.A295S mutant c-actins preferential incorporation in the stress fibre system, whereas the p.R312H and p.E361G mutants showed a more circumferential anti-HA staining suggesting preferred incorporation into short cortical actin filaments. Bars: 50 µm. (E-E´) Transduction of NRCs with adenoviral constructs encoding wt c-actin. (E) Immunostaining with anti-HA antibody (green), (E´) with TRITC-phalloidin (red), and (E´´) merged image also including nuclear staining with Hoechst 33342 (blue). (F,G,I) Merged images of NRCs expressing after transduction the p.A295S, R312H, and E361G mutants, respectively, stained by the identical procedure. Bars: 20 µm.

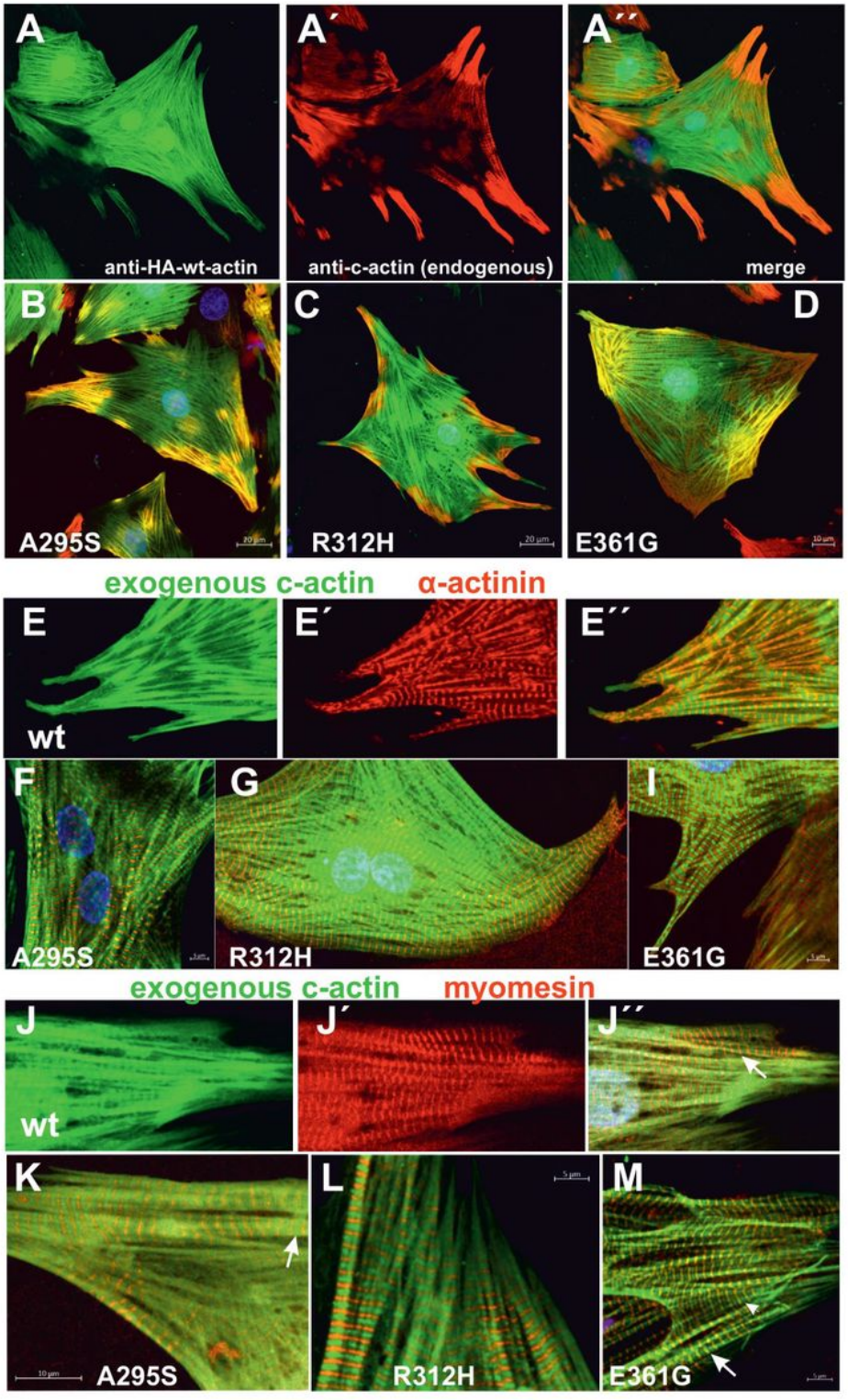


## Figure 8

NRCs expressing HA-tagged c-actin variants counterstained with anti-c-actin mAB. (A) NRCs transduced with adenoviral vector containing HA-tagged wt c-actin stained with anti-HA (green = exogenous) and (A´) with anti-c-actin mAB (red = endogenous), (A´´) merge. Note localisation of endogenous c-actin in cell periphery and extensions. (B) Merged images of identical immunostaining of NRCs infected with HA-tagged p.A295S; (C) p.R312H, and (D) p.E361G. Note partial peripheral co-localisation of endo- and

exogenous c-actin in (B) and (D), whereas in (C) the endogenous c-actin (red) appears more peripherally concentrated without significant co-localising exogenous c-actin. Bars: 20 µm. (E-M) NRCs expressing HA-tagged c-actin variants counterstained with anti-α-actinin or anti-myomesin. (E) NRC transduced with vectors coding wt HA-tagged c-actin stained with anti-HA (green) were counterstained with (E) anti-α-actinin (red) showing cross-striations (arrows). (E´) gives merged image. Note that cross-striation appear in many cases yellowish stained indicating co-localisation (arrows). (F,G,I) gives merged images of identical staining protocol for p.R312H (F), p.A295S (G), and p.E361G (I). Note that in (F) and (C) the cross-striations are yellowish stained indicating also for HA-p.R312H and HA-p.A295S co-localisation with α-actinin suggesting preferred incorporation in the region of the Z-line, i.e. at the plus-ends. In contrast, HA-p.E361G (I) transduced NRCs show a clear separation of the anti-HA (green) and anti-α-actinin immunostaing (red) indicating incorporation at the minus ends in the region of the M-line. (J-J´) Similar immunostaining of wt HA-tagged c-actin (green) and anti-myomesin (red). Note separation of anti-HA and -myomesin in merged image (J´´). (K) merged image for HA-p.A295S and (L) for HA-p.R312H c-actins. Note separation of anti-HA and –myomesin staining in (K and L). In contrast, (M) NRC transduced with HA-p.E361G indicates co-localisation of this c-actin mutant with myomesin supporting the notion that its incorporation into sarcomeric structures occurs at the minus ends (arrow) of existing actin filaments in the region of the M-line. In addition weakly stained anti-HA-immunoreactivity is visible in the middle between the anti-myomesin bands (arrow head). Bars give 20 µm.

## Supplementary Files

This is a list of supplementary files associated with this preprint. Click to download.

- SupplementaryInformation.docx